Two Issues in Wellbore Heat Flow Modelling Along With the Prediction of Casing Temperature in Steam Injection Wells

M. Bahonar, J. Azaiez, and **Z. Chen,** University of Calgary

Abstract

Although several models to determine the formation temperature in the modelling of thermal production and injection processes have already been suggested, there is no rigorous or systematic comparison between these models' predictions that can guide the choice of the most appropriate one. Another issue in thermal wellbore simulators is the commonly used assumption of semisteady-state heat transfer from the wellbore up to the cementing/formation interface. The effect of the semisteady-state assumption vs. the unsteady-state assumption for the heat transfer from the wellbore up to the formation has not received much attention in the literature and can be important in some cases.

The results of a detailed analysis of the two previously described issues can be implemented in all thermal wellbore and reservoir simulators to increase their accuracy.

The previously described stated issues will be addressed in the present work by developing a numerical nonisothermal two-phase wellbore simulator coupled with tubular and cement material and surrounding formation. The first issue will be studied in detail by comparing five different models for the formation temperature treatment (FTT) plugged in the developed thermal wellbore simulator. Investigation of the second issue will be achieved by analyzing the three critical items: first, a 2D heat transfer partial differential equation (PDE) model of the formation is discretized in a general form; second, the gridding system is shifted from the formation toward the casing; and third, an effective specific heat capacity for the casing is used. The effects of choosing different models for FTT and using either the unsteady-state or the semisteady-state assumption in the heat loss from the wellbore up to the formation will be investigated. The model will be validated against field data to show its merits in predicting the casing temperature.

The entire wellbore system contains wellbore, tubing, insulation, annulus, casing, cementing and formation. A fundamental understanding of this system is still a challenging issue in the petroleum industry, and its accurate modelling and coupling with reservoirs has become increasingly significant as more energy resources are sought.

Introduction

Wellbore fluid flow and heat transfer modelling is among the most important tasks in the petroleum industry, particularly now when more complex production, injection, monitoring and testing operations are applied to the wells. Because the wellbore is the only means of communication between the surface and underground, its accurate modelling has a direct and strong impact on the overall design, control and optimization of the reservoir, wells and surface facilities. For these reasons, many investigators have devoted numerous efforts to the wellbore fluid flow and heat transfer modelling for many years.

As early as 1937, Schlumberger et al.[1] pointed out the advantage of fluid temperature measurement in the wellbore. After that, several researchers attempted to estimate the fluid temperature or interpret temperature logs along the wellbore [Nowak[2], Bird[3], Lesem et al.[4], Kirkpatrick[5] and Moss and White[6]]. However, it was in 1962 when the first mathematical model to estimate the fluid temperature as a function of the production time and well depth was proposed by Ramey[7] and Edwardson et al.[8] for hot water injection and mud circulation, respectively.

Ramey's seminal work[7] was based on a number of assumptions to simplify the mass, momentum and heat conservation equations, while weakening the strong coupling between them. In spite of these assumptions, which were necessary to obtain an analytical solution of the problem, this work was the basis of many wellbore flow models [see a detailed literature review on this topic by Bahonar et al.[9]]. Over the last few decades, different researchers [Satter[10], Holst and Flock[11], Willhite[12], Pacheco and Ali[13], Herrera et al.[14], Shiu and Beggs[15], Ali[16], Fontanilla and Aziz[17], Yao[18], Hong and Griston[19], Griston and Willhite[20], Sharma et al.[21], Stone et al.[22], Wu and Pruess[23], Sagar et al.[24], Alves et al.[25] and Hagoort[26]] attempted to relax Ramey's assumptions, model more complex wells and find fast and stable solution methods for solving various wellbore models. Two of those researchers who have had great contributions in the fluid and heat flow modelling of wellbore are Hasan and Kabir, who started their major work by developing an analytical model of the flowing fluid temperature inside the well in 1994[27]. Their work was followed by a series of publications in which the original model has been further modified or applied to other problems [Hasan and Kabir[28], Hasan et al.[29], Hasan and Kabir[30] and Hasan et al.[31]]. Recently, Livescu et al. extended their black-oil nonisothermal multiphase wellbore model, which was submitted for publication in 2008 and accepted in 2010 [Livescu et al.[32]] to the compositional nonisothermal multiphase wellbore model [Livescu et al.[33]]; similar compositional wellbore simulations were also performed by other researchers [Stone et al.[34] and Pourafshary et al.[35]].

A common treatment in the previously stated approaches is that most of them attempted to solve mass, momentum and energy balance equations inside the wellbore. Additionally, a majority of those models coupled the energy balance equation inside the wellbore to the transient formation heat equation by means of an overall heat transfer coefficient. The differences between these approaches were based in the treatment of the formation temperature. For example, some of them solved a 1D or 2D heat transfer PDE in the formation with numerical methods, while others solved various simplified (approximated) 1D heat transfer PDEs of the formation with analytical methods. These different treatments and the resulting different predictions raise questions as to which approach is appropriate for a given process and has correct subsequent effects on the performance of wellbore simulators. An accurate treatment of the formation temperature is important in sensitive processes, such as in the reverse well testing where the surface data are translated back to bottomhole conditions to estimate the formation fluid and rock properties. Therefore, any small error in the calculation of the formation temperature because of its coupling with wellbore equations is boosted along the wellbore and affects all the data obtained at bottomhole conditions.

This paper was accepted for presentation at the Abu Dhabi International Petroleum Exhibition and Conference, Abu Dhabi, UAE, 1–4 November 2010, and revised for publication. Original manuscript received for review 27 June 2010. Revised paper received for review 8 November 2010. Paper peer approved 9 November 2010 as SPE Paper 137134.

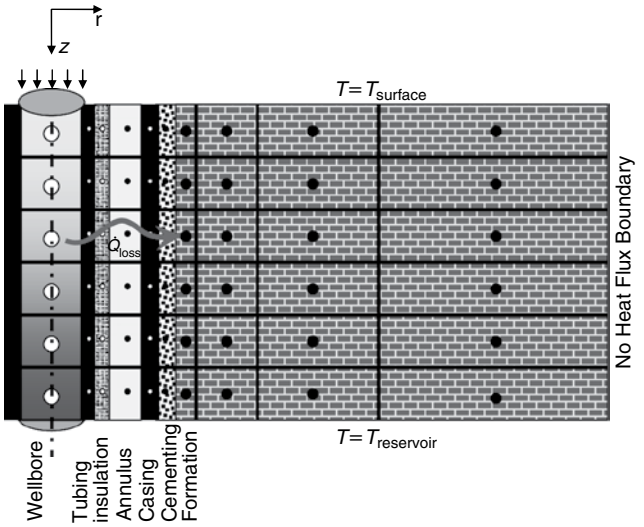

Fig. 1—Schematic representation of the discretized wellbore system and formation, and formation boundary conditions with geometric spacing in radial direction for the formation part.

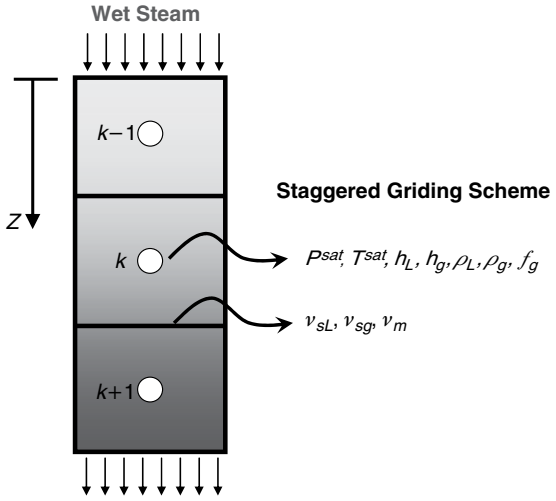

Fig. 2—Schematic representation of the discretized tubing and staggered grid definition (see the positions where different parameters were defined).

Another common strategy in most of the previously mentioned approaches is the semisteady-state assumption for the modelling of heat loss from tubing toward the formation (see the Unsteady-State Heat Transfer Modelling section for more explanation). Although this assumption works well for the later-stage simulation for long-term integration, it is not appropriate for the early-stage simulation or short-term integration when a system is still at the unsteady-state condition. For example, for the reverse well testing where all the events happen within some minutes to some hours, accounting for the transient behaviour is essential to precisely translate wellhead data to the bottomhole conditions.

The objective of this study is to systematically address the two previously described issues. First, a multiphase thermal wellbore model that entails the simultaneous solution of the coupled momentum and mass conservation equations inside the wellbore coupled with an energy conservation equation for the fluids inside the wellbore, surrounding media and formation is briefly described. Then, five different models for FTT are compared. Of these models, two use a numerical method (1D and 2D modelling of the formation) and the other three are based on empirical correlations. Subsequently, the effects of these different FTTs on the evaluation of casing temperature, heat loss, steam quality and wellbore temperature are analyzed. Predictions of the 1D and 2D models of the formation heat transfer are also compared. Additionally, the effect of different choices of FTTs on the run time of a simulator is reported. An approach to consider the unsteady-state heat transfer from the tubing up to cementing/formation interface will be examined and compared with the semisteady-state assumption. Finally, the model proposed is used to predict the casing temperature. Its prediction is compared with both field data and the prediction of other models. The difference in the prediction of the casing temperature between this model and other existing models will be explained in terms of the FTTs that have been used in these models.

Model Formulation

Although the complete formulation of the system shown in **Fig. 1** has been reported in reference [Bahonar et al.[9]], for the sake of this paper, it will be described. For the modelling purpose, this system is divided into three parts: the wellbore tubing, the surrounding system from the tubing wall up to formation and the formation. The equations used for each part and the numerical scheme are briefly described. For more details, the reader may refer to our previous study[Bahonar et al.[9]].

1. Wellbore Tubing. Because the water component in the form of steam or condensate is flowing inside the tubing, the mass balance equation for this component, the pressure drop equation, and the energy balance equation comprise the governing equations.

Mass Balance Equation. The mass conservation equation for the water component is expressed as:

$$-\frac{\partial}{\partial z}\left(\rho_g v_{sg}+\rho_L v_{sL}\right)=\frac{\partial}{\partial t}\left(\rho_m\right) \quad \text{..... (1)}$$

It should be noted that because only the water component exists in the tubing, one mass conservation equation is used.

Momentum Balance Equation. The total pressure drop inside the wellbore tubing is attributed to four major effects: hydrostatic, frictional, acceleration (kinetic) and unsteady-state and can be expressed as [(Beggs and Brill[36], Ali[16], Hasan and Kabir[28], Hasan et al.[29], Hasan et al.[37], Livescu et al.[38,39], Hasan and Kabir[30], Hasan et al.[31], Livescu et al.[33] and Livescu et al.[32]]:

$$-\frac{dp}{dz}=-\frac{\rho_m g\cos(\theta)}{g_c}+\frac{f_m v_m^2 \rho_m}{2d_{ti}g_c}+\frac{\rho_m v_m}{g_c}\frac{dv_m}{dz}+\frac{\rho_m}{g_c}\frac{dv_m}{dt} \quad \text{..... (2)}$$

All parameters are defined in the Nomenclature.

Energy Balance Equation. The energy balance equation for multiphase flow inside the tubing can be expressed as [Ali[16], Hasan and Kabir[28], Hasan et al.[29], Livescu et al.[38,39], Hasan and Kabir[30], Hasan et al.[31], Livescu et al. [33] and Livescu et al.[32]]:

$$\begin{aligned}&-\frac{\partial}{\partial z}\left\{\sum_p\left[\rho_p v_{sp}\left(h_p+\frac{v_p^2}{2g_cJ_c}-\frac{g}{g_cJ_c}\cos(\theta)z\right)\right]-k_f\frac{\partial T_f}{\partial z}\right\}\\&-\frac{Q_{loss_{\Delta z}}}{3600\times A_{ti}}+\frac{m_{H_{\Delta z}}}{A_{ti}}=\left(1+C_T\right)\frac{\partial}{\partial t}\left\{\sum_p\left[f_p\rho_p\left(u_p+\frac{v_p^2}{2g_cJ_c}\right)\right]\right\}\end{aligned} \quad \text{, ... (3)}$$

where J_c is the mechanical equivalent of heat (788 ft-lbf/Btu) and the constant 3,600 converts hours to seconds. In this equation the work done on the fluids by the viscous force is assumed to be small and thus ignored. The term in brackets on the left side accounts for the energy flux because of convection, the work done by the pressure force, the work done on the fluids by the gravitational force and the conductive heat transport (it may become important in the shut-in wells, but will be neglected in our study). The second and third terms on the left side are the rate of heat loss to the surroundings and of heat gain or loss across the perforations, respectively, both per unit length of wellbore. The right-side term is the rate of energy accumulation in the system per unit volume.

The temperature rise of the cement and tubular material may be taken to be a fraction of the rise in the fluid temperature at any time [Hasan and Kabir[28] and Hasan et al.[29]]. In this case, the thermal storage parameter, C_T, represents the capacity of the wellbore to store or release heat as a multiple of the fluid mass and fluid heat capacity. In fact, Hasan and Kabir[28] used the concept of C_T to take into account the unsteady-state heat flow from the tubing up to the formation and assumed that this unsteady-state condition in tubular and cement material is a fraction of unsteady-state in the tubing fluid (C_T is a matching parameter). However, the C_T concept will not be used in our formulation and instead, the unsteady-state condition in the tubular and cement material is modelled with another scheme that will be explained later.

2. Tubular and Cement Material. There is a series of heat resistances from the tubing up to the formation. The heat is lost from the tubing fluid, goes through these heat resistances, and finally is absorbed by the formation as illustrated in Fig. 1. The equation that connects the heat loss, Q_{loss}, from the tubing toward the formation is:

$$\dot{Q}_{loss} = 2\pi r_{to} U_{to} \left(T_f - T_{wb}\right), \quad \text{..... (4)}$$

where U_{to} is the overall heat transfer coefficient given by:

$$\frac{1}{U_{to}} = \frac{r_{to}}{r_{ti} h_f} + \frac{r_{to}\ln\left(r_{to}/r_{ti}\right)}{k_t} + \frac{r_{to}\ln\left(r_{ins}/r_{to}\right)}{k_{ins}} + \frac{r_{to}}{r_{ins}\left(h_c + h_r\right)} + \frac{r_{to}\ln\left(r_{co}/r_{ci}\right)}{k_{cas}} + \frac{r_{to}\ln\left(r_{wb}/r_{co}\right)}{k_{cem}}, \quad \text{..... (5)}$$

where the various parameters are defined in the Nomenclature. The radiation heat transfer coefficient h_r is calculated by the Stefan-Boltzmann law, and the convective heat transfer coefficient is attributed to the Grashof and Prandtl numbers. It is important to know that the controlling resistance over the depth of interest is the convective and radiative heat-transfer coefficients in the annulus that must be honoured appropriately [Hasan and Kabir[30]].

3. Formation. The formation is the part that surrounds the wellbore system and acts as a heat source or sink for the wellbore. Formulations for the formation part will be explained later.

To be able to solve the problem considered, two additional equations are required. The first one is an appropriate equation of state (EOS) to estimate parameters such as fluid density, enthalpy and internal energy. The second one is a set of multiphase flow equations to estimate the in-situ gas volume fraction. Two models, the drift-flux model of Hasan et al.[37] through its simplicity, continuity and differentiability and the Beggs and Brill's model[36] for comparison purposes, are implemented in this study.

Numerical Implementation. **Figs. 1 and 2** illustrate the gridding system used. Staggered gridding (Fig. 2) is used for the tubing part. Because the accumulation term in the earth PDE has the dominant unsteadiness effect on the final solution, all terms containing time in the conservation Equations (1)−(3) are ignored for the tubing. However, the whole system is still at the unsteady-state condition as a result of coupling between the energy Equation (3) inside the tubing and earth PDE through the heat loss Equation (4). In the case that 1D or 2D unsteady-state heat transfer PDEs are used for the FTT, a fully implicit scheme with the finite difference method is used to solve the problem. The formation domain is gridded equally in the axial direction (except the wellhead and bottomhole to capture boundary effects), and geometrically in the radial direction. The resulting system of algebraic equations is solved with BiCGSTAB with an appropriate preconditioner. Detailed information on the formulations, discretization and gridding system of the formation are given in the next section.

Equation (1) with the stated assumption is simplified and for the discretization of both the momentum and energy balances, Equations (2) and (3), the standard Godunov first-order upwinding scheme is implemented. An iterative procedure that involves updating the nonlinear coefficients and overall heat transfer coefficient at each iteration is used for the entire fluid-flow and heat transport computation. The numerical algorithm works in a double-iterative manner on the gas superficial velocity and fluid pressure to solve the three conservation equations sequentially. More details that explain numerical implementation are given in Bahonar et al.[9].

Models for FTT

In this section, five different models for FTT will be presented. The procedure used to calculate the tubing external temperature, the insulation external temperature (if any) and the casing internal temperature as well as that for updating the overall heat transfer coefficient will be first explained. Assuming steady-state heat transfer from fluid inside the tubing up to the cementing/formation interface in each timestep, equations for the temperature calculation of the internal and external surfaces of different parts (tubing, insulation, casing and cementing) can be derived. The casing internal temperature is expressed as:

$$T_{ci} = T_{wb} + \left[\ln\left(\frac{r_{wb}}{r_{co}}\right)\Big/k_{cem} + \ln\left(\frac{r_{co}}{r_{ci}}\right)\Big/k_c\right] r_{to} U_{to}\left(T_f - T_{wb}\right) \quad \text{..... (6)}$$

It is common in the literature to assume that k_c is large ($T_{ci} \approx T_{co}$), which leads to the following simplified equation:

$$T_{ci} = T_{wb} + \left[\ln\left(\frac{r_{wb}}{r_{co}}\right)\Big/k_{cem}\right] r_{to} U_{to}\left(T_f - T_{wb}\right) \quad \text{..... (7)}$$

In the present study, this simplifying assumption will not be adopted and the original Equation (6) will be used. If there is insulation around the tubing, the insulation external temperature is calculated by:

$$T_{ins} = T_f - \left[\ln\left(\frac{r_{ins}}{r_{to}}\right)\Big/k_{ins} + \ln\left(\frac{r_{to}}{r_{ti}}\right)\Big/k_t\right] r_{to} U_{to}\left(T_f - T_{wb}\right) \quad \text{..... (8)}$$

Otherwise, the tubing external temperature is given by:

$$T_{to} = T_f - \left[\ln\left(\frac{r_{to}}{r_{ti}}\right)\Big/k_t\right] r_{to} U_{to}\left(T_f - T_{wb}\right) \quad \text{..... (9)}$$

In each timestep, the tubing (or possibly insulation) external temperature and casing internal temperature are estimated based on the information from the last timestep by use of Equations (6), (8) and (9). Knowing these temperatures, the convective and radiative heat transfer coefficients for the annulus (temperature-dependent) are calculated from the Grashof and Prandtl numbers and Stefan-Boltzmann law, respectively. The overall heat transfer coefficient U_{to} is then obtained from Equation (5). With calculated U_{to}, the tubing (insulation) external temperature and casing internal temperature are recalculated again and after that, the convective and radiative heat transfer coefficients for the annulus as well as U_{to} are updated. This iterative procedure will be repeated until appropriate convergence is gained in the tubing (insulation) external temperature, casing internal temperature and U_{to}.

As seen from Equations (6)−(9), T_f and T_{wb} are present in all these equations and should be updated at each timestep. T_f is obtained by solving the coupled mass, momentum and energy balance equations inside the main computational loops. After computing this new fluid temperature and by use of the old formation temperature, the heat loss from the wellbore toward the formation can be obtained by use of Equation (4).

The next step of updating the formation temperature represents a major part of the present study and will be examined lengthily. There are two main approaches to update the unsteady-state formation temperature. The first one involves solving numerically the 1D or 2D PDE of heat transfer in the formation with appropriate

boundary and initial conditions at the expense of high computational time and complex modelling. In the second approach, simpler and faster correlations that are based on approximations of the 1D heat transfer PDE of the formation are used. Obviously, the solution of the numerical approach is more physically meaningful than that of the correlating approach. The different models for FTT are presented next.

FTT Models No. 1 and 2

The 2D heat transfer PDE (FTT No. 1) is given by:

$$\frac{1}{r}\frac{\partial}{\partial r}\left(k_{er}r\frac{\partial T_e}{\partial r}\right)+\frac{\partial}{\partial z}\left(k_{ez}\frac{\partial T_e}{\partial z}\right)=\frac{1}{\alpha_e'}\frac{\partial T_e}{\partial t}, \quad \text{..... (10)}$$

where α_e' is defined as:

$$\alpha_e'=\frac{1}{\rho_e C_{pe}} \quad \text{..... (11)}$$

In Equations (10) and (11) T_e is the formation (earth) temperature, k_{er} the conduction coefficient in the radial direction, k_{ez} the conduction coefficient in the z-direction, ρ_e the formation density and C_{pe} the heat capacity of the formation.

The initial condition given by the following equation is simply a multilinear increase in the formation temperature from the surface to the reservoir with a slope of g_{T_l} that is the geothermal gradient of the formation for layer "l":

$$T_{ei_l}=T_{ei_{wh\,l}}+g_{T_l}z\cos(\theta_l) \quad \text{..... (12)}$$

The four boundary conditions as depicted in Fig. 1 are given by:

$$T_e=T_{surface} \quad at \quad z=0,\ r\geq r_{wb}, \quad \text{..... (13)}$$

$$T_e=T_{reservoir} \quad at \quad z=L,\ r\geq r_{wb}, \quad \text{..... (14)}$$

$$\frac{\partial T_e}{\partial r}=0 \quad at \quad 0\leq z\leq L, \quad r\to\infty, \quad \text{..... (15)}$$

$$\dot{Q}_{loss}=-2\pi r k_e\frac{\partial T_e}{\partial r} \quad at \quad 0\leq z\leq L, \quad r=r_{wb} \quad \text{..... (16)}$$

That is, the top and bottom boundaries of the formation remain at a constant temperature, there is no heat flux at the outer earth boundary and the heat flux is prescribed at the cementing/earth interface.

The 1D heat transfer PDE (FTT No. 2) is given by:

$$\frac{1}{r}\frac{\partial}{\partial r}\left(k_{er}r\frac{\partial T_e}{\partial r}\right)=\rho_e C_{pe}\frac{\partial T_e}{\partial t}, \quad \text{..... (17)}$$

with the same initial and boundary conditions as in 2D except that Equations (13) and (14) are irrelevant in this case.

Equation (10) for the 2D case can be discretized in a fully implicit scheme as:

$$\alpha_L T_{k-1,\,i}^{n+1}+\alpha_W T_{k,\,i-1}^{n+1}+\alpha_C T_{k,\,i}^{n+1}+\alpha_E T_{k,\,i+1}^{n+1}+\alpha_U T_{k+1,\,i}^{n+1}=-T_{k,\,i}^{n}, \quad \text{..... (18)}$$

where the coefficients, α_L, α_W, α_C and α_V are given in Appendix A. Equation (18) can be rearranged in matrix form as [A][B]=[C], where [A] is a five-diagonal matrix of coefficients, [B] is the vector of unknowns and [C] is the vector of the known parameters. α_L, α_W, α_C, α_E and α_A are lower, west, central, east and upper diagonals of matrix [A]. In the 1D case, α_L and α_U are zero and α_C does not contain the z-terms.

In the case where $k_{er}=k_{ez}=k_e$, Equation (10) can be simplified to:

$$\frac{1}{r}\frac{\partial}{\partial r}\left(r\frac{\partial T_e}{\partial r}\right)+\frac{\partial^2 T_e}{\partial z^2}=\frac{\partial^2 T_e}{\partial r^2}+\frac{1}{r}\frac{\partial T_e}{\partial r}+\frac{\partial^2 T_e}{\partial z^2}=\frac{1}{\alpha_e}\frac{\partial T_e}{\partial t}, \quad \text{..... (19)}$$

where α_e is the earth thermal diffusion coefficient:

$$\alpha_e=\frac{k_e}{\rho_e C_{pe}} \quad \text{..... (20)}$$

Even though this assumption ($k_{er}=k_{ez}=k_e$) was made in our previous work [Bahonar et al.[9]], using the more general Equation (10) has a number of benefits. First, it allows handling the multilayer formation with different geothermal gradients and different initial temperatures. Second, in the case that the casing becomes hot, it may cause some of the water in the formation near the casing to vaporize and move away from the casing. This causes some of the formation around the casing to dry; therefore, the thermal conductivity of the formation near the casing will decrease and can subsequently cause a significant increase in the casing temperature and possible casing failure [Willhite[12]]. With the more general form of the formation equation this phenomenon can be accurately modelled.

It is worth mentioning that in the axial direction an equal gridding system is used, except near wellhead and bottomhole locations where more refined grids are adopted to capture boundary effects. A geometric gridding system is used in the radial direction. The number of grids and the maximum radius of the formation that is assumed as infinity where the initial temperature remains fixed are arbitrary (in this study we assume r_e=50 ft and the number of grids=15). The locations of grid boundaries and centres for the geometric gridding system are given in Appendix B. The resulting equations are solved by use of the BiCGSTAB method with an appropriate preconditioner for acceleration.

FTT Model No. 3

The second approach of FTT is based on the correlations that approximate the 1D heat transfer Equation (17) with the assumption of $k_{er}=k_e=$ constant. Ramey[7] used the following equation to calculate the heat loss toward the formation:

$$\frac{Q_{loss}}{\Delta z_k}=\frac{2\pi k_e\left(T_{wb}-T_e\right)}{f(t)}, \quad \text{..... (21)}$$

where f(t) is a dimensionless time function. Combining the previously described expression with the original heat loss equation and by use of the equation for the initial formation temperature [Equations (22) and (23), respectively], Equation (24) can be derived for the cementing/formation interface temperature (known as the wellbore temperature, T_{wb}):

$$\frac{Q_{loss}}{\Delta z_k}=2\pi r_{to}U_{to}\left(T_f-T_{wb}\right), \quad \text{..... (22)}$$

$$T_e=T_{surface}+g_T Z, \quad \text{..... (23)}$$

$$T_{wb}=\frac{r_{to}U_{to}f(t)T_f+k_e T_e}{r_{to}U_{to}f(t)+k_e} \quad \text{..... (24)}$$

Now, if we can somehow obtain f(t) and plug it in Equation (24), the updated formation temperature can be obtained. In fact, Equation (17) has an exact solution [Wang[40]] as given by:

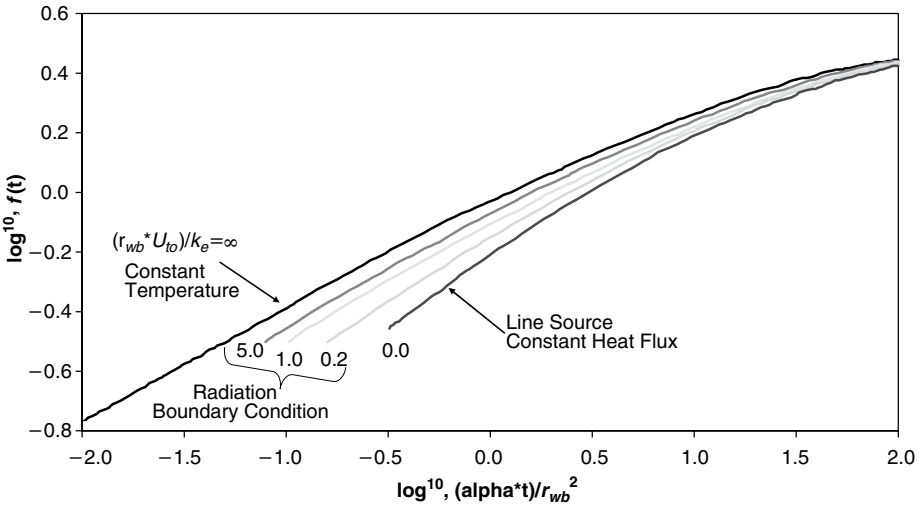

Fig. 3—Dimensionless time function vs. dimensionless time[42].

$$f(t)=\frac{-2I}{\pi}, \quad \text{..... (25)}$$

$$I=\int_0^{\infty}\frac{1-e^{-u^2 t_D}}{u^2}\frac{Y_1(u)J_0(u)-Y_0(u)J_1(u)}{J_1^2(u)+Y_1^2(u)}du \ , \quad \text{..... (26)}$$

where

$$t_D=\frac{\alpha_e t}{r_{wb}^2} \quad \text{..... (27)}$$

In Equation (26), J_0, J_1, Y_0 and Y_1 are the Bessel and modified Bessel functions of zero and first order, respectively. However, solving the integral Equation (26) even numerically is difficult. Ramey[7] suggested the following approximate correlation for f(t):

$$f(t)=\ln\left[\frac{2\sqrt{(\alpha t)}}{r_{wb}}\right]-0.29 \quad \text{..... (28)}$$

The previously described expression for f(t) is called Ramey's dimensionless time function. This function has been frequently used by many investigators [Pacheco and Ali[13], Herrera et al.[14], Horne and Shinohara[41], Fontanilla and Aziz[17] and Yao[18]].

FTT Model No. 4

Fontanilla and Aziz [Fontanilla[42] and Fontanilla and Aziz[17]] estimated the dimensionless time function f(t) from solutions for radial heat conduction in an infinitely long cylinder. They obtained the solutions based on Ramey's[7] and Carslaw and Jaeger's[43] work as shown in **Fig. 3** that presents f(t) for a cylinder losing heat at constant temperature, a constant heat flux line source and a cylinder losing heat under radiation or convection boundary conditions [Fontanilla[42]]. Fig. 3 shows that all five solutions converge to a single line that is the line source solution for time greater than 1 week. In fact, Ramey's dimensionless time function is an approximation for the line source solution that works for time greater than 1 week. Fontanilla[42] used a regression technique to obtain third-order polynomial approximations for each of the five curves in Fig. 3, which are more general than Ramey's single equation. The five third-order polynomial approximations are as follows:

D=0 or the line source solution (Ramey's type solution, good for time greater than 1 week):

$$f(t)=10^{-0.19865+0.48034\times t_D-0.08619\times t_D^2+0.00148\times t_D^3}\approx\ln\left[\frac{2\sqrt{(\alpha t)}}{r_{wb}}\right]-0.29 \ , \quad \text{.....(29)}$$

$$D\le 0.2: f(t)=10^{-0.12557+0.38757\times t_D-0.07525\times t_D^2+0.01065\times t_D^3} \ , \quad \text{..... (30)}$$

$$D\le 1.0: f(t)=10^{-0.08738+0.3689\times t_D-0.04619\times t_D^2-0.00222\times t_D^3} \ , \quad \text{..... (31)}$$

$$D\le 5.0: f(t)=10^{-0.03018+0.36166\times t_D-0.06586\times t_D^2-0.00393\times t_D^3} \ , \quad \text{..... (32)}$$

$$D>5.0: f(t)=10^{-0.02435+0.33116\times t_D-0.033723\times t_D^2-0.00525\times t_D^3} \ , \quad \text{..... (33)}$$

where t_D is the dimensionless time defined as:

$$t_D=\log_{10}\left(\frac{\alpha\times t}{r_{wb}^2}\right), \quad \text{..... (34)}$$

and

$$D=\frac{r_{wb}U_{to}}{k_e} \quad \text{..... (35)}$$

FTT Model No. 5

The last dimensionless time function to consider is the one introduced by Hasan and Kabir[27]:

$$f(t)=1.1281\sqrt{t_D}\left(1-0.3\sqrt{t_D}\right) \qquad if \quad 10^{-10}\le t_D\le 1.5, \quad \text{.....(36)}$$

$$f(t)=\left[0.4063+0.5\ln(t_D)\right](1+0.6/t_D) \qquad if \quad t_D>1.5 \quad \text{..... (37)}$$

The previously described expressions for f(t) are discontinuous at t_D=1.5. Therefore, they suggested another form for f(t) [Hasan and Kabir[27]]:

TABLE 1—SUMMARY OF DIFFERENT FTT MODELS		
FTT Model No.	FTT Model Type	FTT Model Name
1	Numerical	2D model
2	Numerical	1D model
3	Analytical	Ramey's model
4	Analytical	Fontanilla and Aziz's model
5	Analytical	Hasan and Kabir's model

$$f(t) = \ln\left[e^{-0.2t_D} + \left(1.5 - 0.3719e^{-t_D}\right)\sqrt{t_D} \right] \quad \text{..... (38)}$$

This form has been frequently used by Hasan and Kabir in their recent works.

Table 1 clearly summarizes the stated five FTT models in terms of the model number, type and name and can be referred to at any time. In the next section, we will check the performance of each of these models in terms of prediction and computational time.

Results

Effects of Different Choices of FTT. We now examine the effect of different choices of FTT on the performance of a wellbore simulator. The data for running the simulator as shown in **Table 2** are chosen from the Field Tests 1A from a test on the 61-0 Martha Bigpond well [Bleakley[44]]. **Figs. 4−7** demonstrate the effect of the FTT type on the estimation of temperature of the cementing/formation interface for 1, 10, 100 and 1,000 hours of steam injection, respectively. In these figures, our base and accurate solution is the numerical 2D modelling because it is the closest to the physics of the problem. As seen in Fig. 4, Ramey's model gives an unrealistic result for 1 hour of steam injection because it predicts a temperature of the cementing/formation interface less than the geothermal formation temperature that is the initial temperature of the formation. For the case of 10 hours, Ramey's model still underpredicts the temperature 7.9°F or a 8.8% relative error in average for this field test (Fig. 5). As reported in Fontanilla[42], Yao[18] and Hagoort[26], Ramey's model works quite well for a large time (more than a week). Therefore, this model is the second most accurate one next to the 2D modelling for 100 and 1,000 hours of steam injection. Hasan's model predictions are quite acceptable for the first three cases with approximately 5.2%−5.9% relative errors with respect to the 2D model; its relative error rises to 18.9% for the last case. It seems that among the correlations, Fontanilla and Aziz's model has a normal behaviour, starting with a 8.5% relative error for 1 hour of steam injection and decreasing to 7.7%, 7.6% and 6.0% relative errors as time progresses.

Next, the effect of a temperature difference for the estimation of the cementing/formation interface temperature with different models on the casing temperature, heat loss, steam quality and tubing fluid temperature is discussed. For this purpose, the results of the simulator for 1,000 hours of steam injection by plugging different models for FTT are depicted in **Figs. 8 – 11.** Fig. 8 shows the maximum relative errors of 2.6% – 3.2% from the basecase in the estimation of the casing temperature at bottomhole and wellhead conditions, respectively, because of choosing different models of FTT. The relative errors in the estimation of heat loss, steam quality and tubing wellbore temperature at bottomhole conditions are 9.5%, 0.9% and approximately 0.0%, respectively (Figs. 9−11). As seen from these figures, the maximum and minimum effects are observed in the heat loss and tubing fluid temperature, respectively. The result that the tubing fluid temperature is not sensitive to the type of the FFT model can be explained by the fact that different formation temperature estimations increase or decrease the heat loss, but as long as the fluid inside the tubing is in the two-phase region, the steam quality fluctuates and amends the heat loss change accordingly. Therefore, the tubing fluid temperature remains almost constant. It should be mentioned that if the field input data are changed, the effect of choosing different types of FTT will be different from that reported here. For instance, if the steam injection flow rate decreases, the difference in prediction of the formation temperature by different models will affect the prediction of other parameters more significantly.

Because the difference in prediction of the formation temperature between the 1D and 2D numerical modelling appears near the wellhead and bottomhole locations (they predict almost the same formation temperature in other locations), their performance is compared just for the wellhead in **Table 3** for different times of steam injection (starting from 1 hour up to 10,000 hours). As seen from this table,

TABLE 2—FIELD DATA PARAMETERS FOR FIELD TESTS 1A–1B, 3A–3B AND 3C–3E*			
	Field Test 1A–1B	Field Test 3A–3B	Field Test 3C–3E
r_{ti}, ft	0.088500	0.12465	0.12465
r_{to}, ft	0.104167	0.145833	0.145833
r_{ins}, ft	No insulation	No insulation	No insulation
r_{ci}, ft	0.166667	0.265000	0.265000
r_{co}, ft	0.187500	0.291667	0.291667
r_{wb}, ft	0.600000	0.411667	0.411667
k_e, Btu/(hr ft °F)	1	1.36	1.36
α_e, ft²/hr	0.0286	0.04	0.04
g_T, °F/ft	0.0283	0.0037	0.012
k_{cem}, Btu/(hr ft °F)	0.2	0.417	0.417
ε_{to}, dimensionless	0.9	0.9	0.9
ε_{ci}, dimensionless	0.9	0.9	0.9
$\dot{w}$, lbm/hr	4,850	14,600	14,600
χ, fraction	0.8	0.7	0.7
p_{wh}, psia	250	950	1,350
T_{wh}, °F	50	50	70
Depth, ft	1,600	2,700	2,700
Annulus pressure, psia	14.7	1,200	1,200

* Fontanilla and Aziz[17]

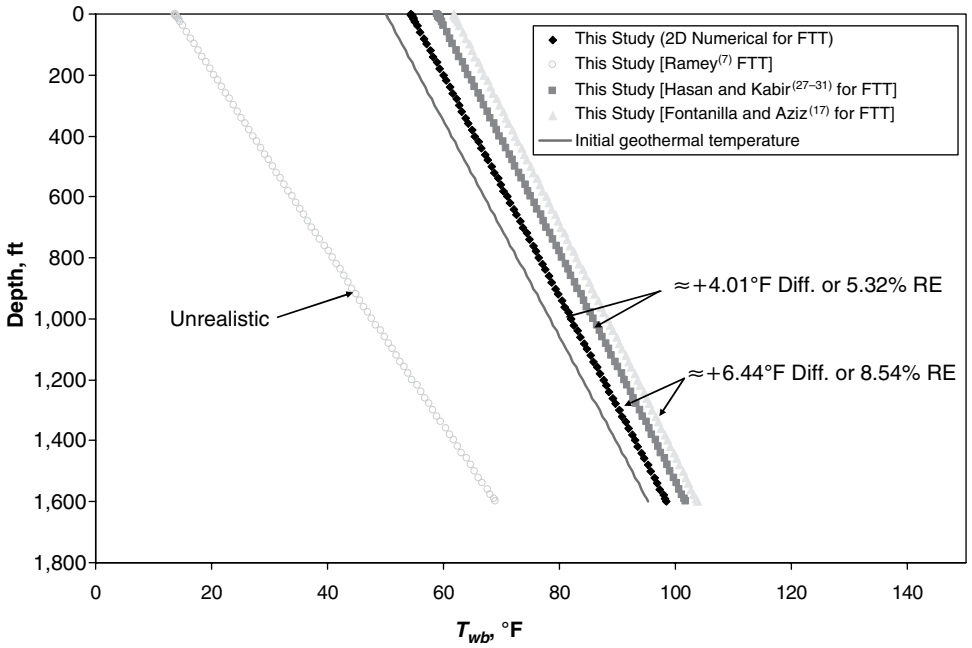

Fig. 4—Prediction of wellbore temperature vs. depth for 1 hour of steam injection using different methods for FTT.

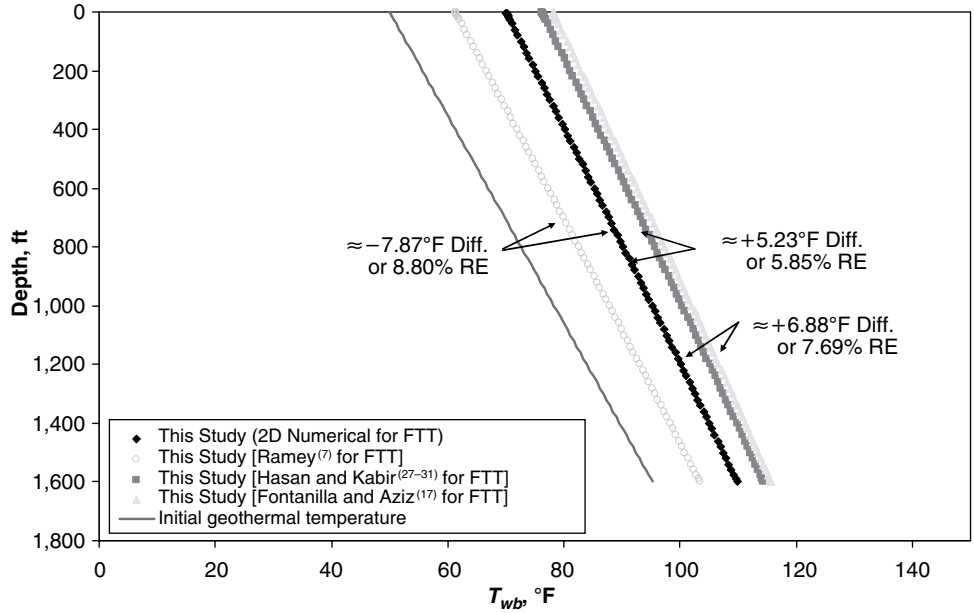

Fig. 5—Prediction of wellbore temperature vs. depth for 10 hours of steam injection using different methods for FTT.

as time goes on, the difference between the predictions of these two models increases and also diffuses more and more from the wellhead toward the depth of the wellbore. Note that this difference increases in the case where a colder surface and/or hotter bottomhole temperature exists or where the axial heat conductivity in the formation is higher than the radial heat conductivity.

To compare the run time between different approaches, Field Test 1 is run for 71 hours of steam injection with 0.5 hour as the timestep with the multiphase flow methods of Hasan et al.[37] and Beggs and Brill[36] (the results are reported in **Table 4**). When the method of Hasan et al.[37] is used for multiphase flow equations, the correlations for FTT are the fastest with approximately 54 seconds of run time on average, as expected; the 1D and 2D numerical modelling approaches require approximately 78 and 92 seconds of run time, respectively. If Beggs and Brill's multiphase flow correlations[36] are used instead, the run time reduces 8 seconds on average in all cases of FTT. This is because the use of an internal iteration in the Hasan et al.[37] method to correct the initial guess for the friction factor that increases the run time compared with Beggs and Brill's method[36].

Among the main drawbacks of the correlations is that they are ascending functions in terms of time. Therefore, if some interruption occurs in any injection or production operation (for instance, shut in the well), they cannot predict the formation temperature correctly unless a new geothermal temperature gradient is calculated near the wellbore, which will introduce an additional approximation and also a time-dependent parameter. Another possible remedy is the use of the superposition principle in the analytical models that requires storage of data from previous timesteps. On the other hand, the 1D and 2D numerical modelling approaches have the capability to adjust themselves to any change in the wellbore operation (increasing or decreasing the flow rate in injection

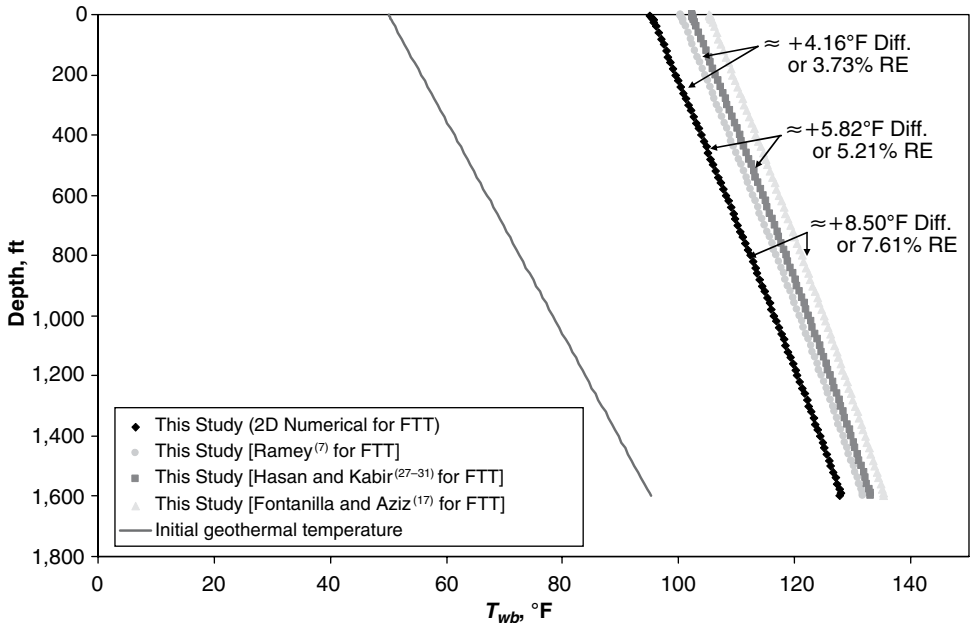

Fig. 6—Prediction of wellbore temperature vs. depth for 100 hours of steam injection using different methods for FTT.

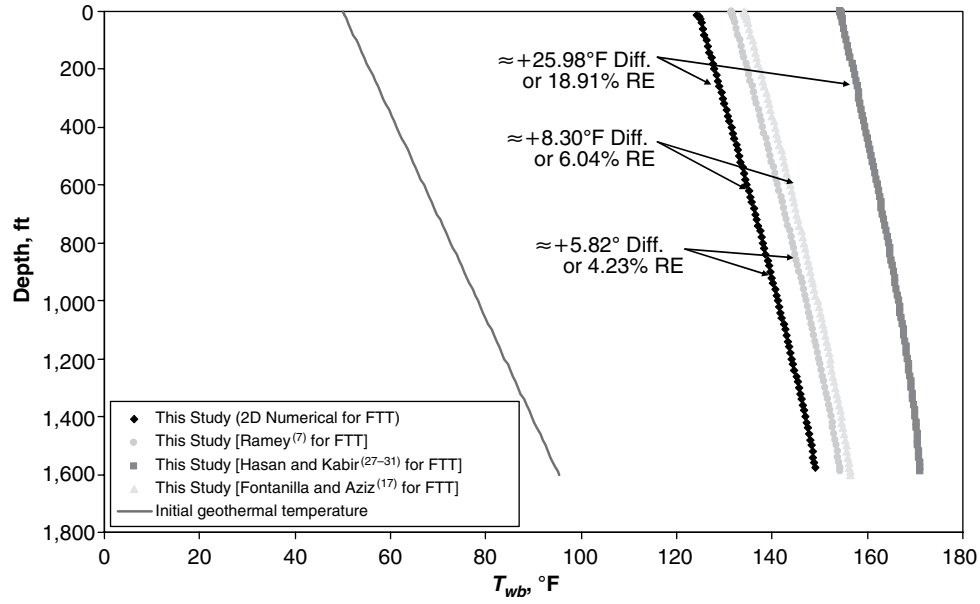

Fig. 7—Prediction of wellbore temperature vs. depth for 1,000 hours of steam injection using different methods for FTT.

or production wells or shut in the well for multiple times). Overall, it is recommended to use the 2D numerical modelling for FTT in the processes that require an accurate wellbore modelling. For example, in the reverse well testing with surface data, where these data must be accurately translated back to the bottomhole condition without entering additional errors, the multiphase methods impose some errors; if the heat transfer modelling also has some error, the quality of data that will be obtained at the bottomhole condition will decrease. The 2D approach can also be used when an accurate standalone wellbore simulator is required. In the case where quick and less accurate results (particularly for the simulation of several wells in a full-field reservoir simulation) are required, using the correlations for FTT is recommended.

Unsteady-State Heat Transfer Modelling. In our previous work [Bahonar et al.(9)] and so far in this paper, the heat transfer from the wellbore up to the cementing/formation interface has been assumed at the semisteady-state condition, which means that the tubing wall (possible insulation), annulus fluid, casing wall and cementing are all assumed not to have any heat capacity to absorb the heat and to be at the steady-state condition in each timestep. This assumption works well for long steam injecting operations because the heat absorbed by the wellbore system (from the tubing wall up to the cementing/formation interface) is negligible compared with the total heat injected into the reservoir. However, the heat capacity of these materials will be important in the transient regime when any small heat loss affects all the results. None of the models in the literature have treated the heat loss from the tubing up to the cementing/formation interface in the fully unsteady-state mode. The reason is that in the wellbore annulus we have all sorts of highly nonlinear and coupled heat transfer mechanisms, including conduction, convection and thermal radiation. Additionally, because the annulus is not a porous medium, computational fluid dynamic (CFD) techniques must be used to model this part in the fully unsteady-state mode. However, because modelling an annulus with a depth of 1,000 ft by

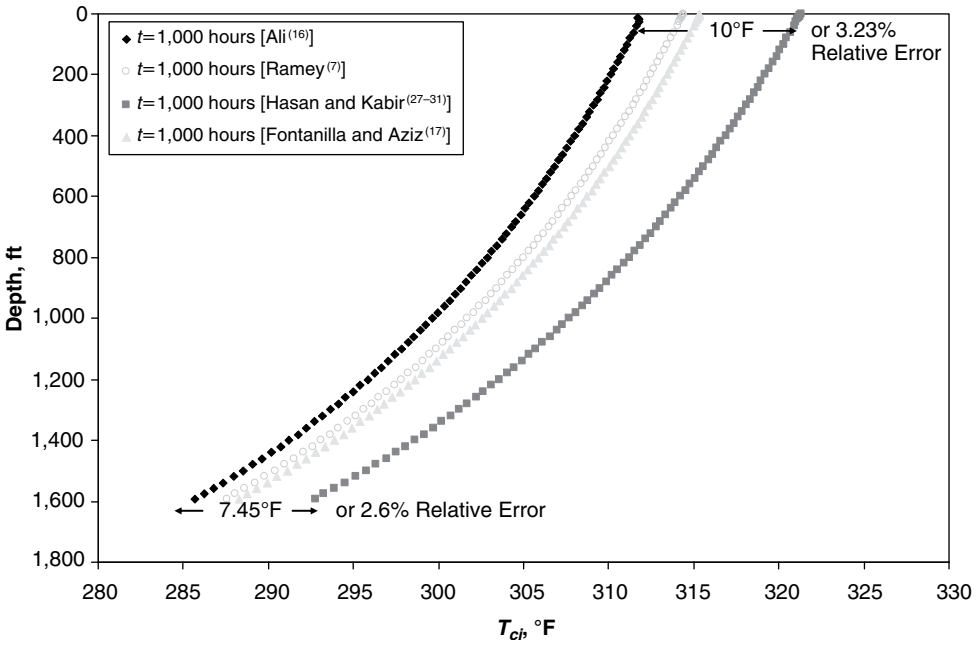

Fig. 8—Effect of FTT on the prediction of casing temperature.

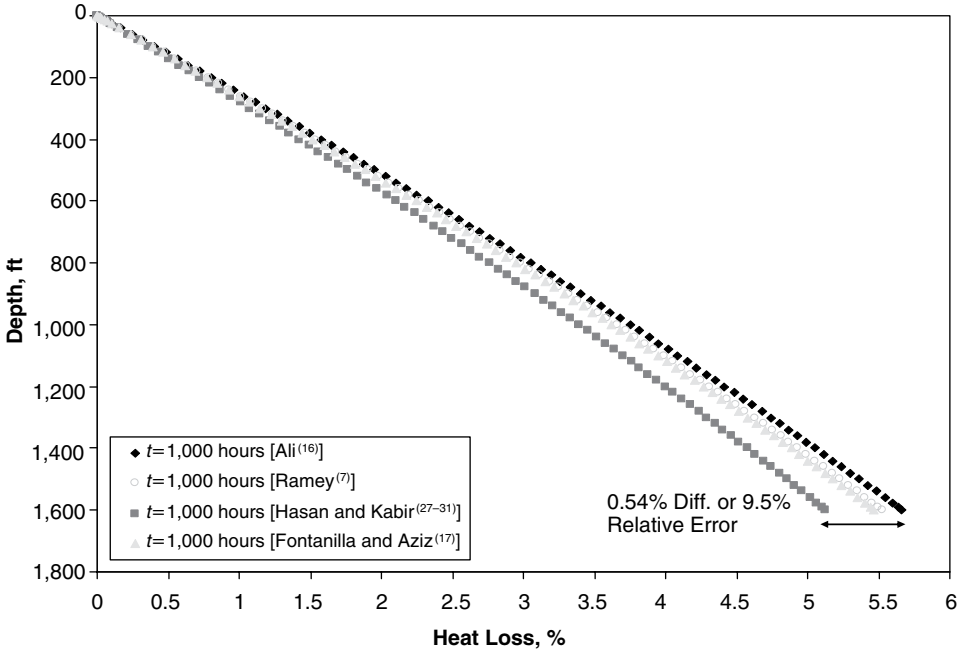

Fig. 9—Effect of type of FTT on the prediction of cumulative heat loss.

the CFD techniques is extremely expensive in terms of computational time, no model uses this approach. To achieve some benefits from both the fully unsteady-state mode in terms of accuracy and the semisteady-state in terms of computational speed, we introduce a new scheme and call it the semiunsteady-state mode, which is explained now.

As noted earlier, in this paper a more general discretization form of the 2D numerical model for FTT is used. This model enables to handle any heterogeneity in the heat conductivity in both the radial and axial directions. Therefore, the grid systems are shifted from the formation toward the casing. This implies that instead of starting from the cement/formation interface, gridding starts from casing, then covers all over the cementing and finally ends on the formation. The heat capacity of the tubing wall and annulus gas (the gas heat capacity and its density are negligible compared with the large heat capacity and density of the tubing and casing walls) is absorbed into the casing heat capacity by considering an effective heat capacity as indicated by Equation (39):

$$C_{P,\,eff} = \begin{pmatrix} \rho_{tubing} V_{tubing} C_{P,\,tubing} \\ +\rho_{annulus} V_{annulus} C_{P,\,annulus} \\ +\rho_{casing} V_{casing}\ C_{P,\,casing} \end{pmatrix} \Big/ \rho_{casing}\, V_{casing}, \quad \text{..... (39)}$$

where V is the volume of each component shown by its index.

Simulations with Field Test 1 as the input data are run for 1, 71 and 168 hours of steam injection with two different options. The first option is running the simulator with discretizing the formation and assuming the semisteady-state heat condition in the wellbore system in each timestep (from the tubing wall up to the cementing/

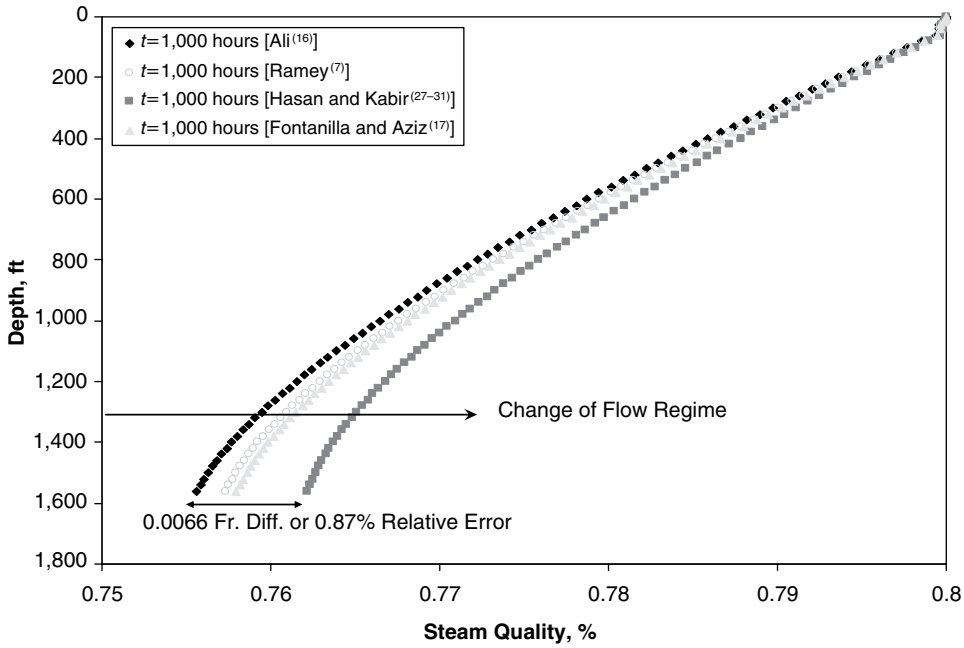

Fig. 10—Effect of type of FTT on the prediction of utilized steam quality.

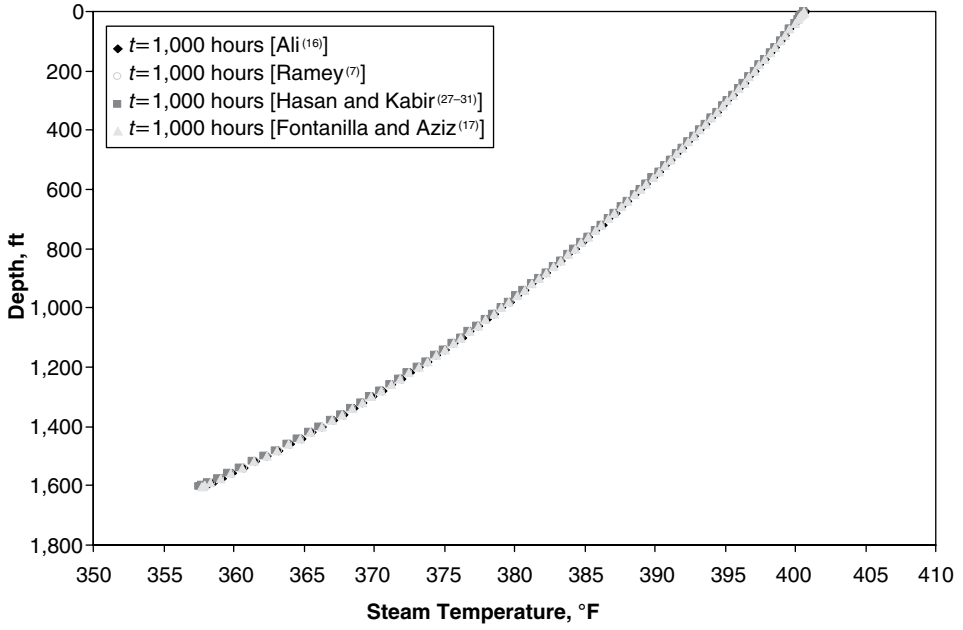

Fig. 11—Effect of type of FTT on the prediction of tubing fluid temperature.

formation interface). The second option that has been recently introduced is to consider semiunsteady-state heat transfer in the wellbore system. The temperature distributions for these two options and the initial formation temperature at depth of 800 ft and within 1 ft of the wellbore radius are depicted in **Figs. 12−14.** As seen from these figures, the differences between the results of these two options are considerable at small time of steam injection and decrease as time increases. For example, the casing temperature difference for these two options at this depth is 31.4°F for 1 hour of steam injection and decreases to 20°F and 18.9°F for 71 and 168 hours of steam injection, respectively. Therefore, it is recommended to use the semisteady-state scheme for almost all field applications except in the case where initial results (transient time) are required and important.

Prediction of Casing Temperature. In this section, our wellbore simulator is used to predict the casing temperature. Its performance is checked against both field data and predictions of other models. The main idea here is to show how using different models for FTT may affect the prediction of the casing-temperature profile in short times. The field data used are acquired from reference [Herrera et al.(14)] and are for the 38-25 William Holding well of the Cat Canyon field. This well is a deep steam injector at a depth of 2,700 ft where the cyclic steam stimulation (CSS) process was used before a steam drive pilot was started. A thermocouple was installed at the depth of 2,700 ft in this well to monitor the casing temperature and the results of this monitoring are illustrated in **Fig. 15.** In the first and second cycles of the CSS process, two and three casing measurements were acquired, respectively, that for consistence with reference [Fontanilla and Aziz(17)] are referred to as 3A, 3B, 3C, 3D and 3E with 16, 168, 240, 276 and 312 hours of steam injection, respectively. The field data used in the simulation is reported in Table 2.

TABLE 3—EFFECT OF 1D OR 2D FTT ON THE PREDICTION OF WELLBORE TEMPERATURE AT DIFFERENT TIMES

	Time=1 hr			Time=10 hrs			Time=100 hrs		
Depth, ft	T_{wb} 1D, °F	T_{wb} 2D, °F	Diff., °F	T_{wb} 1D, °F	T_{wb} 2D, °F	Diff., °F	T_{wb} 1D, °F	T_{wb} 2D, °F	Diff., °F
0	50	50	0	50	50	0	50	50	0
0.75	54.03	53.95	0.07	70.21	67.74	2.48	95.33	78.85	16.49
2.25	54.07	54.07	0.00	70.25	70.18	0.07	95.37	92.13	3.23
4.75	54.14	54.14	0.00	70.31	70.31	0.00	95.42	95.12	0.30
8.25	–	–	–	70.40	70.40	0.00	95.50	95.48	0.01
12.75	–	–	–	–	–	–	95.60	95.59	0.00
18.875	–	–	–	–	–	–	95.73	95.73	0.00
26.25	–	–	–	–	–	–	95.89	95.89	0.00
40	–	–	–	–	–	–	–	–	–
60	–	–	–	–	–	–	–	–	–
80	–	–	–	–	–	–	–	–	–
100	–	–	–	–	–	–	–	–	–
120	–	–	–	–	–	–	–	–	–

TABLE 3—EFFECT OF 1D OR 2D FTT ON THE PREDICTION OF WELLBORE TEMPERATURE AT DIFFERENT TIMES (CONT)

	Time=1,000 hrs			Time=10,000 hrs		
Depth, ft	T_{wb} 1D, °F	T_{wb} 2D, °F	Diff., °F	T_{wb} 1D, °F	T_{wb} 2D, °F	Diff., °F
0	50	50	0	50	50	0
0.75	124.53	83.20	41.33	148.57	84.35	64.22
2.25	124.56	104.65	19.90	148.60	108.09	40.51
4.75	124.60	116.72	7.88	148.63	123.81	24.83
8.25	124.66	122.27	2.40	148.68	133.85	14.83
12.75	124.74	124.21	0.53	148.75	140.18	8.57
18.875	124.85	124.79	0.07	148.83	144.52	4.31
26.25	124.98	124.98	0.01	148.94	146.86	2.08
40	125.23	125.23	0.00	149.14	148.72	0.42
60	125.58	125.58	0.00	149.42	149.37	0.06
80	–	–	–	149.71	149.70	0.01
100	–	–	–	150.00	150.00	0.00
120	–	–	–	150.28	150.28	0.00

As seen in Table 2, the only differences between the two sets of field data are the geothermal temperature gradient and wellhead pressure. The geothermal temperature gradient originally reported by Herrera et al.[14] was 0.012°F/ft for both cycles of the process. The geothermal temperature gradient was decreased from 0.012°F/ft to 0.0037 °F/ft by Fontanilla and Aziz[17], resulting from deficiency in FTT that was in the Fontanilla and Aziz model. As mentioned previously, the correlations for FTT do not work for the case that some interruptions occur in the well unless the geothermal temperature gradient is modified accordingly (which is a trial and error procedure until a new and good matching number for the geothermal temperature gradient can be found). For this reason and because the well was under the injection of steam for 1 week before soak and production started, the geothermal temperature gradient was decreased from 0.012°F/ft (for the second cycle) to 0.0037°F/ft (for the first cycle). This means that the formation was initially at a lower temperature, but after the first cycle it warmed up. The wellhead pressure in the field was also increased from 950 psi to 1,350 psi from the first to the second injection cycles.

Figs. 16–20 show the prediction of the casing temperature by both our model [with the two multiphase flow equations of Hasan et al.[37] and Beggs and Brill[36]] and Fontanilla and Aziz's

TABLE 4— EFFECT OF DIFFERENT FTT MODELS ON THE RUN TIME OF THE WELLBORE SIMULATOR

FTT Model No.	FTT Model Type	FTT Model Name	Run Time, seconds	Remarks
1	Numerical	2D model	91.7	1.70 times slower
2	Numerical	1D model	78.4	1.46 times slower
3	Analytical	Ramey's model	54.2	
4	Analytical	Fontanilla and Aziz's model	53.7	
5	Analytical	Hasan and Kabir's model	53.6	

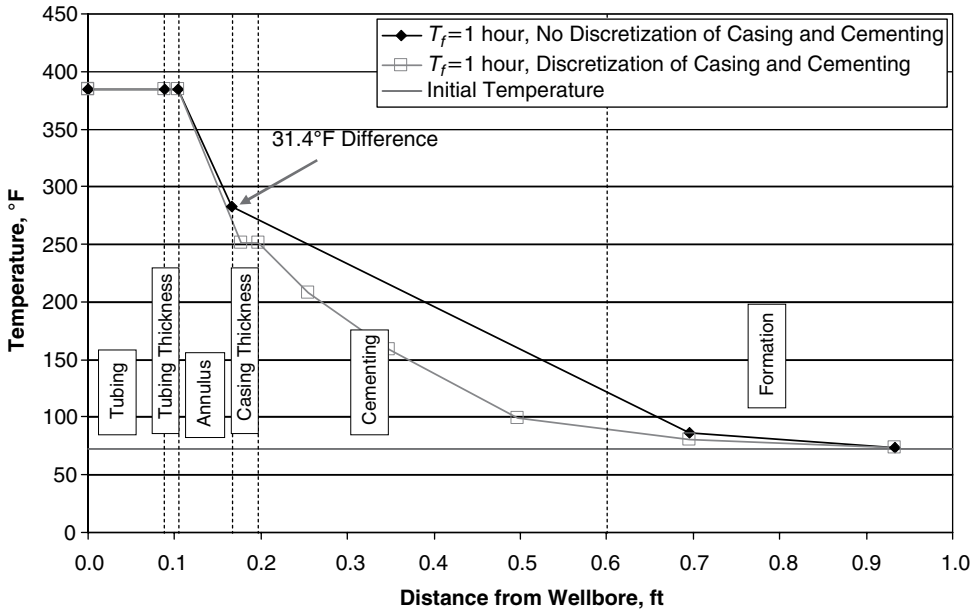

Fig. 12—Comparison of prediction of temperature near the wellbore between using semisteady-state and semiunsteady-state assumption for heat flow from tubing toward the formation after 1 hour of steam injection.

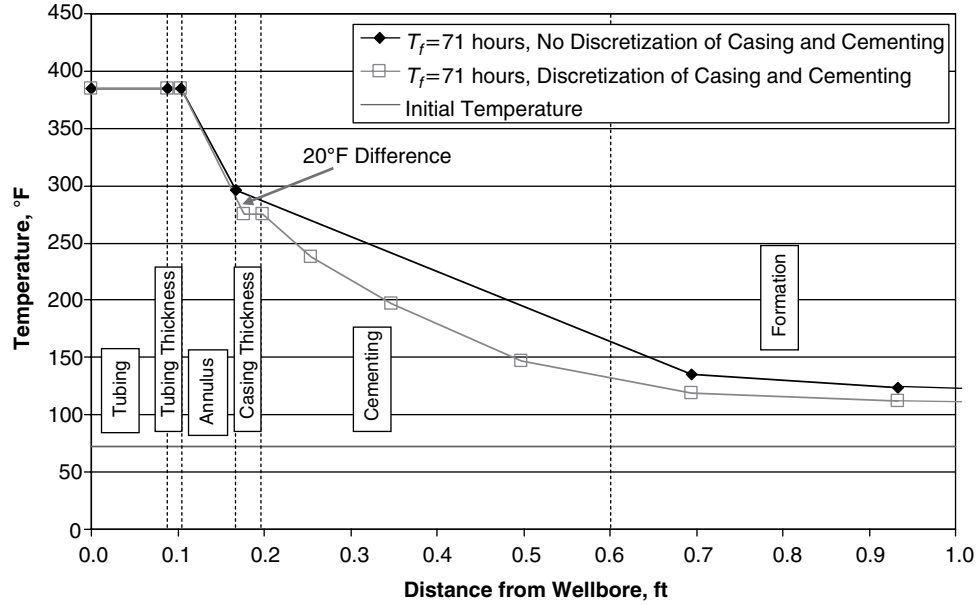

Fig. 13—Comparison of prediction of temperature near the wellbore between using semisteady-state and semiunsteady-state assumption for heat flow from tubing toward the formation after 71 hours of steam injection.

model[17] [with the two multiphase flow equations of Aziz et al.[45] and Beggs and Brill[36]]. As seen from these figures, Fontanilla and Aziz's model[17] with the Aziz et al. correlations[45] underpredicts the casing temperature in all cases with approximately 5°F in the first and 8°F in the second cycles, while the same model with the Beggs and Brill correlations[36] gives a good prediction of the casing temperature in all cases. Our model with the Hasan et al. correlations[37] gives a match with less than 1°F difference in all cases except for the Field Test 3B, where the difference is near 5°F. Additionally, our model based on the Beggs and Brill correlations gives a match with less than 2°F difference in all cases except for the Field Test 3A where the difference is again near 5°F. One interesting point that can be detected from these figures is that in all cases the bottomhole trend of the curves are toward the field casing temperature, but the starting point in the wellhead for our model is different from that of the Fontanilla and Aziz model in Field Tests 3A and 3B. This difference decreases from 3A to 3B and disappears after a long injection time. The reason again goes back to the use of a correlation for FTT in the Fontanilla and Aziz model that has some errors at early time, and this error decreases at sufficiently later time. Because our model is based on a 2D numerical model for FTT, it shows correct trends for the casing temperature prediction.

Fig. 21 shows the steam pressure change inside the wellbore vs. depth by different models for Field Test 1A. This figure illustrates that there is a large difference between the predictions of the different models (except those that use the same multiphase flow correlations).

Figs. 22 and 23 demonstrate steam quality and heat loss vs. depth for Field Test 1A, respectively. Both models with different multiphase equations predict almost the same numbers: a steam quality decrease from 70% to approximately 40% and heat loss of near 20%. Although the large pressure differences were observed for different models (Fig. 21), similar steam quality and

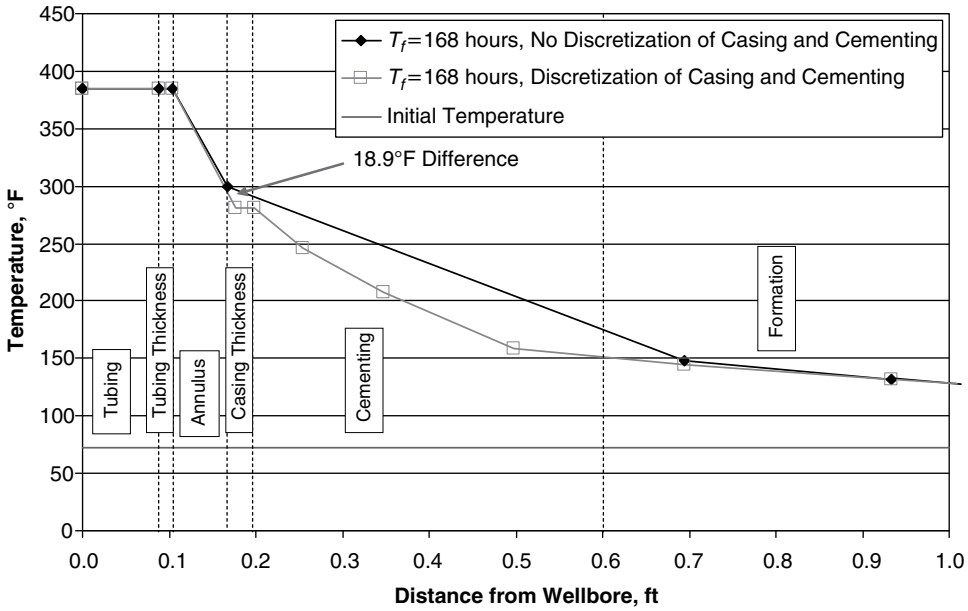

Fig. 14—Comparison of prediction of temperature near the wellbore between using semisteady-state an semiunsteady-state assumption for heat flow from tubing toward the formation after 168 hours of steam injection.

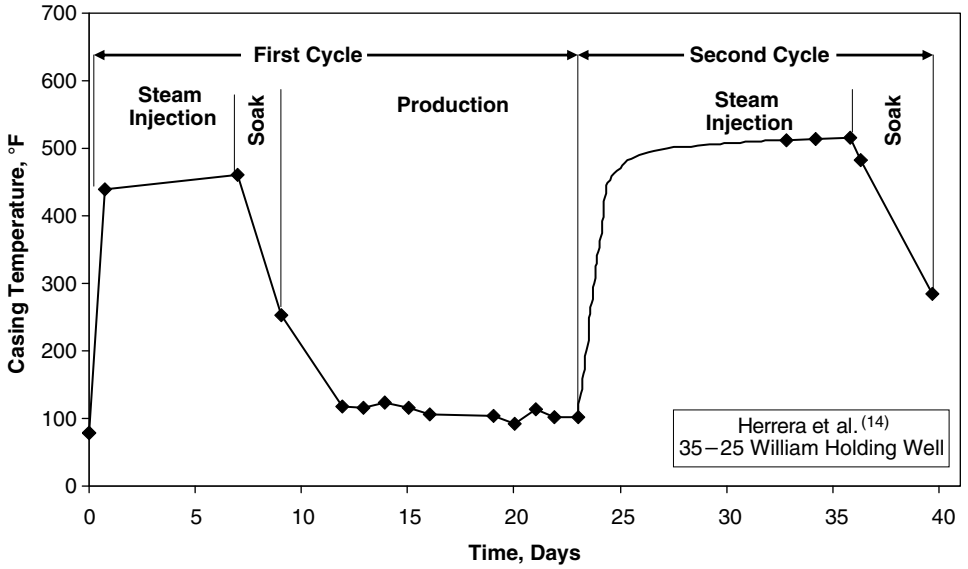

Fig. 15—Casing temperature vs. time at the depth of 2,700 ft for the cyclic steam stimulation of Field Tests 3A−3E [Herrera et al.(14)].

heat loss are predicted. The reason is that the steam injection mass flow rate is high (14,600 lbm/hr) for this field test; therefore, steam quality and heat loss are not affected by the differences in the prediction of the various models. These differences were large in Field Tests 1A, 1B and 2 with lower injection mass flow rates [Bahonar et al.(9)]. One reason for the high heat loss (20%) for this well is the high-pressure annulus of 1,200 psia (this high-pressure annulus captured with an appropriate real high-pressure fluid model inside the annulus) that boosts the convective heat loss from the tubing toward the formation. Using a packer to isolate the annulus and decrease its pressure and also using insulation in wells similar to this one are the possible solutions to decrease the heat loss.

Figs. 24 and 25 compare the steam quality and heat loss vs. depth for Field Tests 1A and 1B. As seen in these two figures, as more steam is injected into the reservoir (a longer time of steam injection) and the well surrounding medium grows warmer, the steam quality increases and heat loss decreases with time.

Conclusions

A 2D formation heat-transfer PDE has been discretized implicitly in a more general form to be able to treat any heterogeneity in the formation heat properties in both the radial and axial directions. Applications include the modelling of multilayer formation with multiple geothermal temperature gradients and the modelling of water evaporation in the formation near the casing to more accurately estimate the casing temperature.

Five different models, including two numerical (1D and 2D PDEs) and three analytical models (correlations) for FTT, have been studied, and the effect of choosing any of them on the performance of a wellbore simulator has been investigated. It has been seen that using the numerical 2D model for FTT gives the best results in expense of more computational time. This model is recommended for accurate processes such as reverse well testing and for the applications that require a standalone wellbore simulator. For longer time and faster simulation runs, with several wells in a full field simulation, the implementation of correlations for FTT is ad-

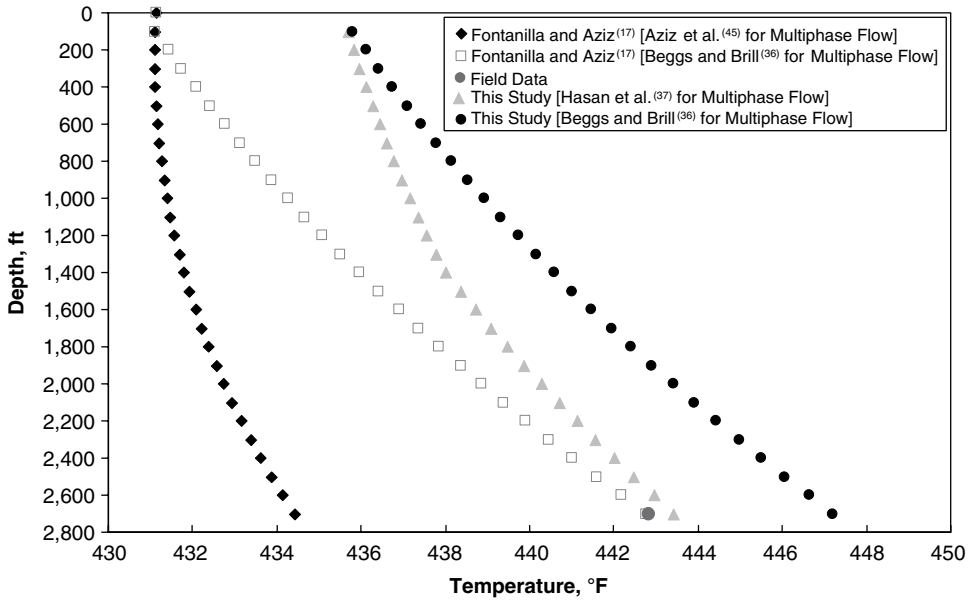

Fig. 16—Validation of numerical results against Field Test 3A and comparison of predicted casing temperature with other models after 16 hours of steam injection.

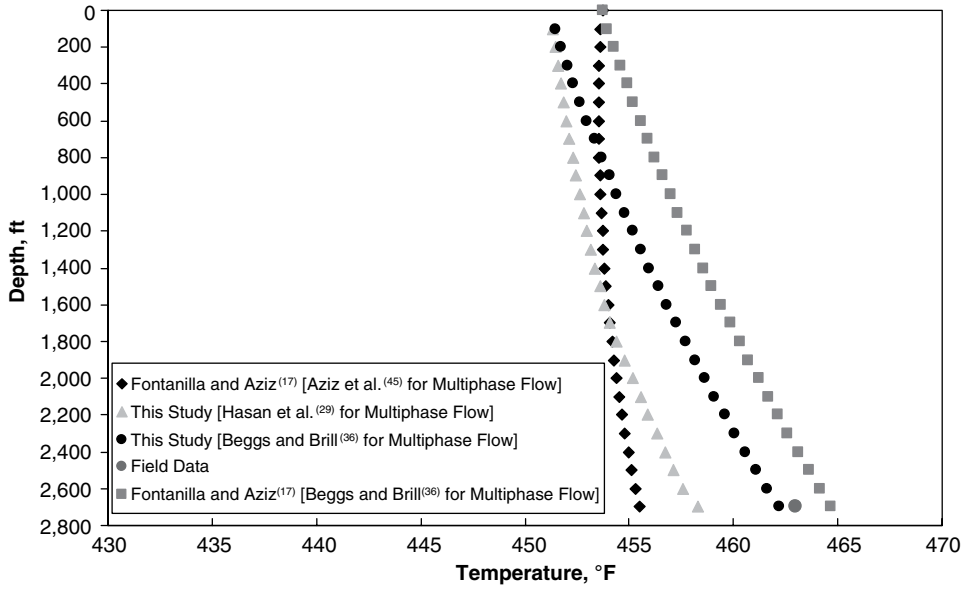

Fig. 17—Validation of numerical results against Field Test 3B and comparison of predicted casing temperature with other models after 168 hours of steam injection.

vised. Both 1D and 2D heat transfer PDEs give good results, but as time progresses the prediction power of the 1D model decreases compared with the 2D one, especially at the top and bottom well boundaries. Among the correlations, Ramey's model[7] works the best for time greater than a week, Fontanilla and Aziz's model[17] performs reasonably well for all time with decreasing errors as time becomes large, and Hasan's model[27] works well for all time but with less accuracy at significantly large times.

An approach has been presented to consider the unsteady-state condition from tubing up to formation. It has been observed that the assumption of semisteady-state (in contrast to semiunsteady-state) heat transfer in the tubular and cement materials is a good assumption for long time processes. The difference between these two assumptions in predicting temperatures of different parts in the wellbore system decreases as time becomes large.

The model has been successfully validated against field data and the prediction of other models and shown to accurately predict the casing temperature. The differences in the prediction of the casing temperature profile between using our model and other models, specifically at small times, have been explained in terms of the FTT type used in each model.

Acknowledgements

The authors would like to thank the Alberta Ingenuity, now part of Alberta Innovates–Technology Futures, for funding this research project. **JCPT**

Nomenclature

A_g = area occupied by gas, ft^2
A_{ti} = inside tubing area, ft^2

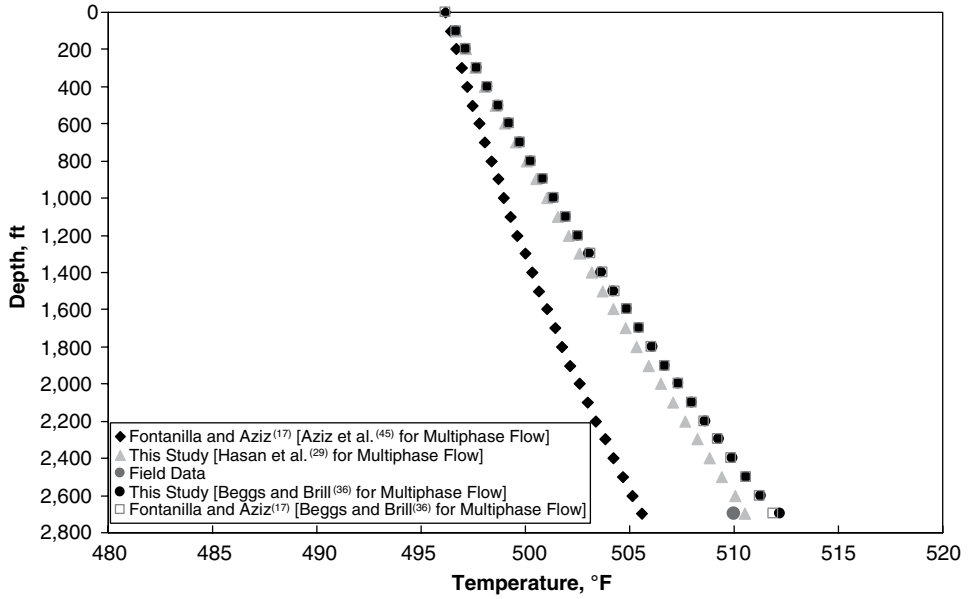

Fig. 18—Validation of numerical results against Field Test 3C and comparison of predicted casing temperature with other models after 240 hours of steam injection.

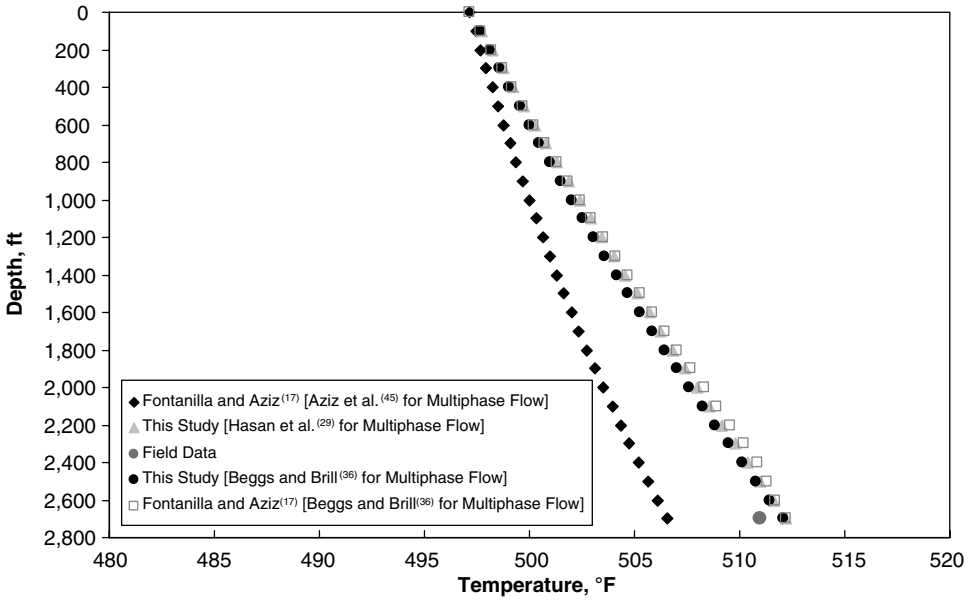

Fig. 19—Validation of numerical results against Field Test 3D and comparison of predicted casing temperature with other models after 276 hours of steam injection.

C_o = distribution coefficient in the drift-flux model, dimensionless
C_p = heat capacity, Btu/(lbm °F)
C_{pe} = earth heat capacity, Btu/(lbm °F)
C_{peff} = effective heat capacity, Btu/(lbm °F)
C_T = thermal storage parameter, dimensionless
d_{ti} = internal tubing diameter, ft
D = dimensionless parameter defined in Equation (35), dimensionless
f_g = gas in-situ volume fraction, dimensionless
f_L = liquid in-situ volume fraction, dimensionless
f_m = Moody friction factor, dimensionless
g = acceleration because of gravity, 32.17 ft/s^2
g_c = gravitational conversion constant, 144×g, lbm/lbf×in^2/ft^2×ft/s^2
g_T = geothermal gradient, °F/ft
h_c = convective heat transfer coefficient of fluid inside annulus, Btu/(hr ft^2 °F)
h_f = convective heat transfer coefficient of fluid, Btu/(hr ft^2 °F)
h_g = gas enthalpy, Btu/lbm
h_L = liquid enthalpy, Btu/lbm
h_p = enthalpy of phase p (liquid water or steam), Btu/lbm
h_r = radiative heat transfer coefficient of fluid inside annulus, Btu/(hr ft^2 °F)
k_{cas} = thermal conductivity of casing, Btu/(hr ft °F)
k_{cem} = thermal conductivity of cementing, Btu/(hr ft °F)
k_e = thermal conductivity of earth, Btu/(hr ft °F)
k_{er} = radial thermal conductivity of earth, Btu/(hr ft °F)
k_{ez} = vertical thermal conductivity of earth, Btu/(hr ft °F)
k_f = thermal conductivity of fluid, Btu/(hr ft °F)
k_{ins} = thermal conductivity of insulation, Btu/(hr ft °F)

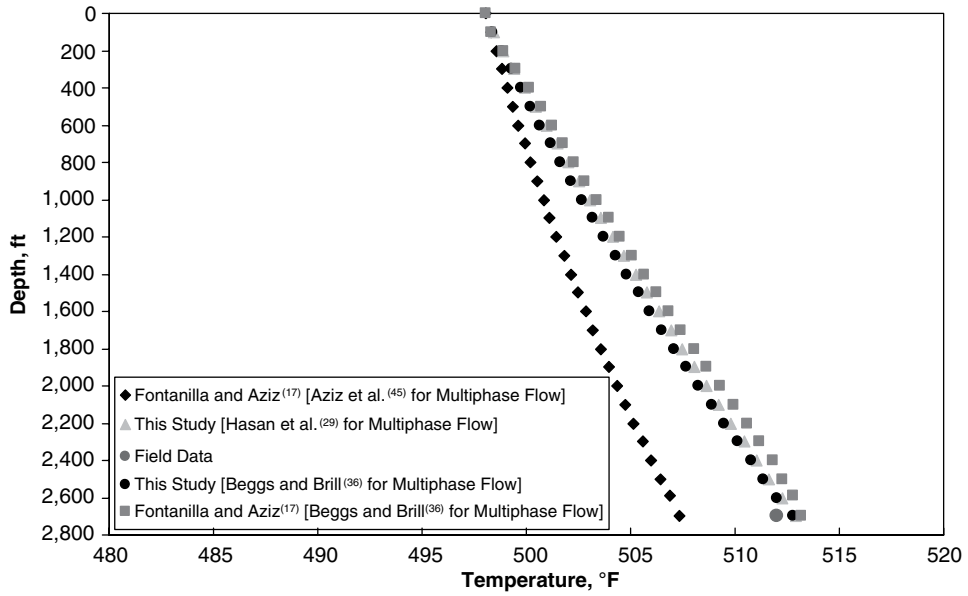

Fig. 20—Validation of numerical results against Field Test 3E and comparison of predicted casing temperature with other models after 312 hours of steam injection.

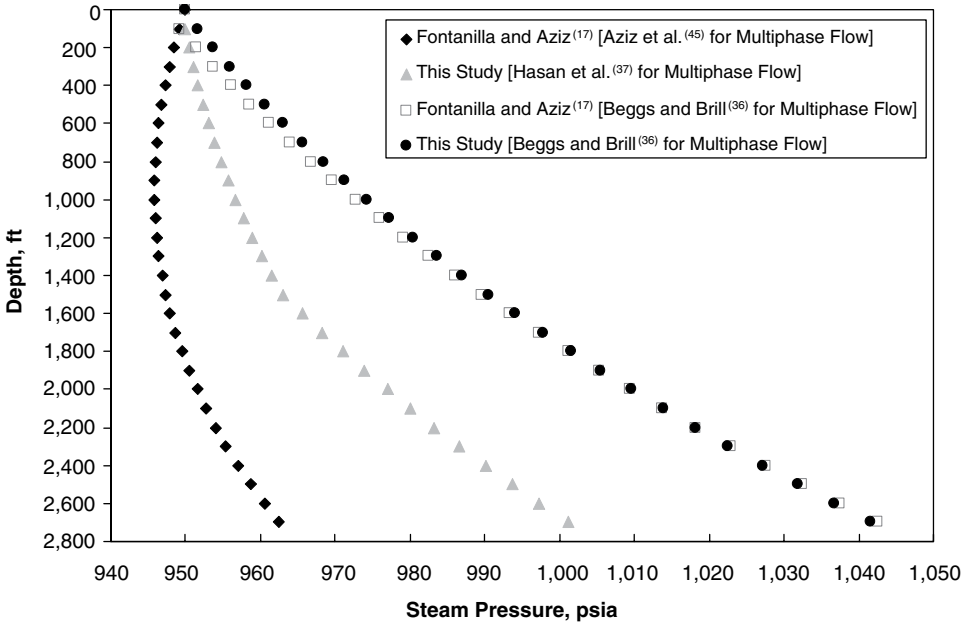

Fig. 21—Comparison of predicted steam pressure with other models for Field Test 3A after 16 hours of steam injection.

k_t = thermal conductivity of tubing, Btu/(hr ft °F)
L = total depth of well, ft
$m_{H\Delta x}$ = heat transfer rate across the perforations, Btu/(hr ft)
P = wellbore pressure, psia
P_{wh} = wellhead injection steam pressure, psia
$\dot{Q}_{loss}$ = heat loss rate to surroundings, Btu/(hr ft)
r = radius, ft
r_{ci} = inside radius of casing, ft
r_{co} = outside radius of casing, ft
r_{ins} = radius of the outside insulation surface, ft
r_{ti} = inside radius of tubing, ft
r_{to} = outside radius of tubing, ft
r_{wb} = cementing/formation interface radius, ft
t = time, second (hour)
t_D = dimensionless time, dimensionless
T_{ci} = casing inside temperature, °F
T_{co} = casing outside temperature, °F
T_e = earth temperature, °F
T_{ei} = initial earth temperature, °F
$T_{ei_{wh}}$ = initial wellhead temperature, °F
T_f = fluid temperature inside tubing, °F
T_{ins} = insulation outside temperature, °F
$T_{reservoir}$ = reservoir temperature, °F
$T_{surface}$ = surface temperature, °F
T_{ti} = tubing inside temperature, °F
T_{to} = tubing outside temperature, °F
T_{wb} = cementing/formation interface temperature, °F
T_{wh} = wellhead ambient temperature, °F
u_p = internal energy of phase p (liquid water or steam), Btu/lbm
U_{to} = overall heat transfer coefficient, Btu/(hr ft^2 °F)
v_g = gas velocity, ft/s
v_L = liquid (water) velocity, ft/s
v_m = mixture velocity, ft/s
v_{sg} = superficial gas (steam) velocity, ft/s
v_{sL} = superficial liquid (water) velocity, ft/s

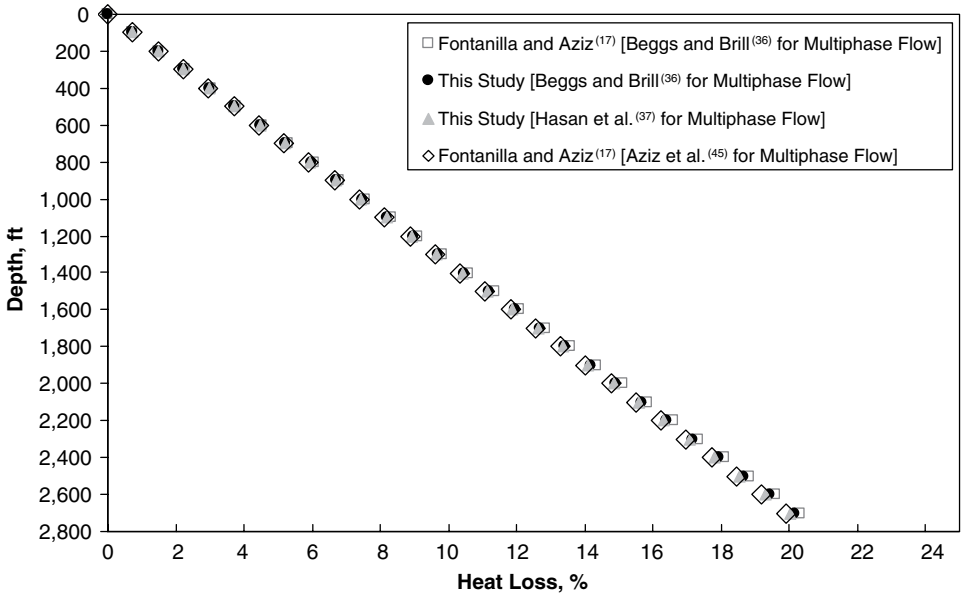

Fig. 22—Comparison of predicted cumulative heat loss with other models for Field Test 3A after 16 hours of steam injection.

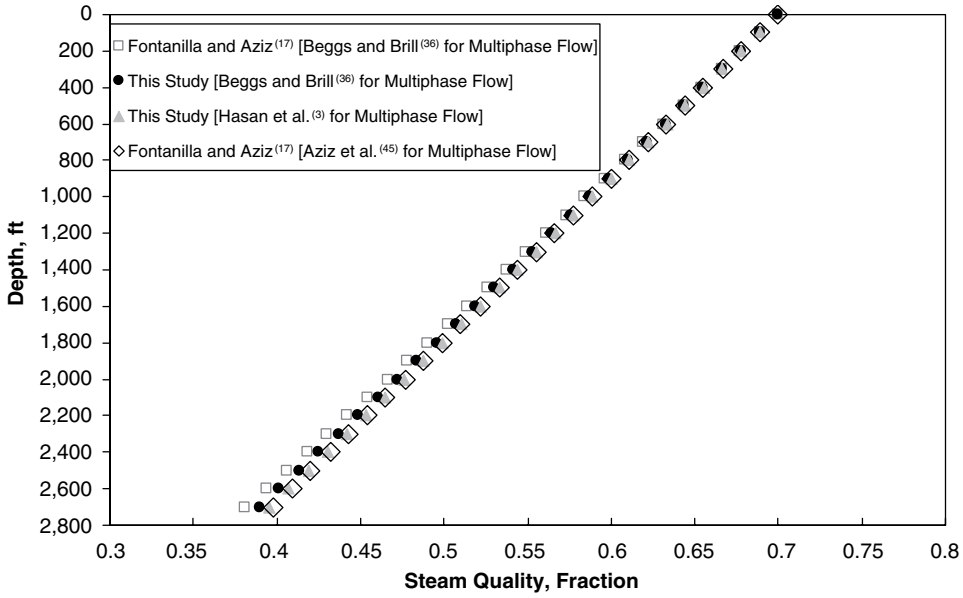

Fig. 23—Comparison of predicted steam quality with other models for Field Test 3A after 16 hours of steam injection.

v_∞ = drift velocity of gas (steam) in liquid (water), ft/s
V = volume, ft^3
$\dot{w}$ = mass flow rate, lbm/hr
x = steam quality, fraction
z = wellbore direction, ft
α_e = formation thermal diffusivity, ft^2/hr
α_e' = parameter defined in Equation (11), (°F ft^3)/Btu
β = growth factor in geometrical gridding system, dimensionless
Δr = radial interval, ft
Δz = distance interval, ft
ε_{ci} = emissivity of inside casing surface, dimensionless
ε_{to} = emissivity of outside tubing surface, dimensionless
θ = local angle between well and the vertical direction, radian
ρ_e = earth density, lbm/ft^3
ρ_g = gas density, lbm/ft^3
ρ_L = liquid density (water density), lbm/ft^3
ρ_m = mixture density, lbm/ft^3

Subscript

k = grid discretization index in the z-direction
l = lth layer in the formation
P = phase p, $p=L$ (liquid) or $p=g$ (gas)
sat = saturation
wh = wellhead

Superscript

n = time discretization index

SI Metric Conversion Factors

Btu	×	1.055056	E+00	= kJ
ft	×	3.048*	E−01	= m
ft^2	×	9.290304*	E−02	= m^2
°F		(°F−32)/1.8		= °C
in.	×	2.54*	E+00	= cm

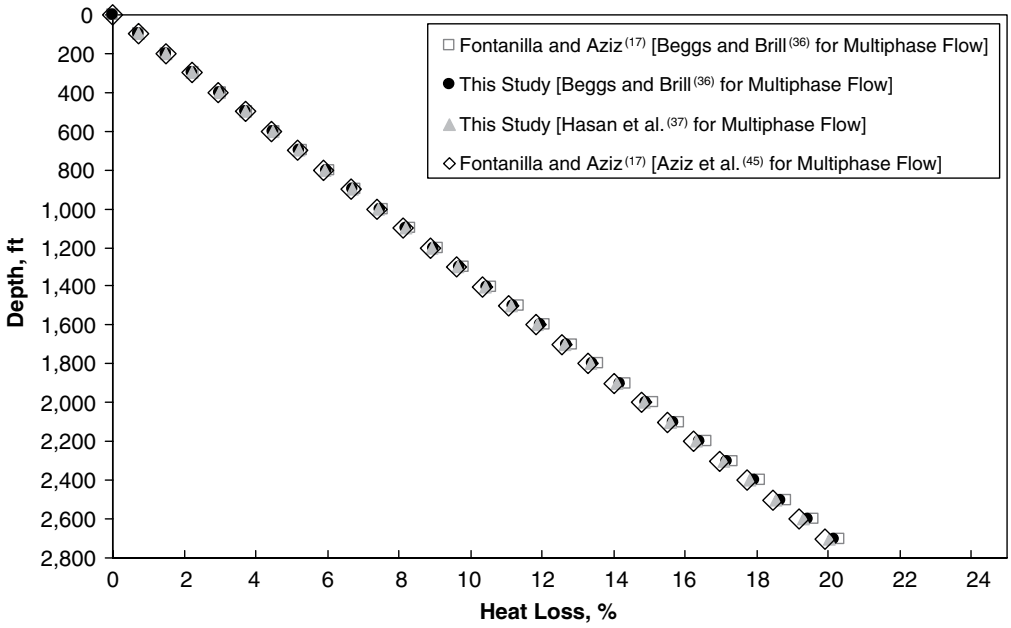

Fig. 22—Comparison of predicted cumulative heat loss with other models for Field Test 3A after 16 hours of steam injection.

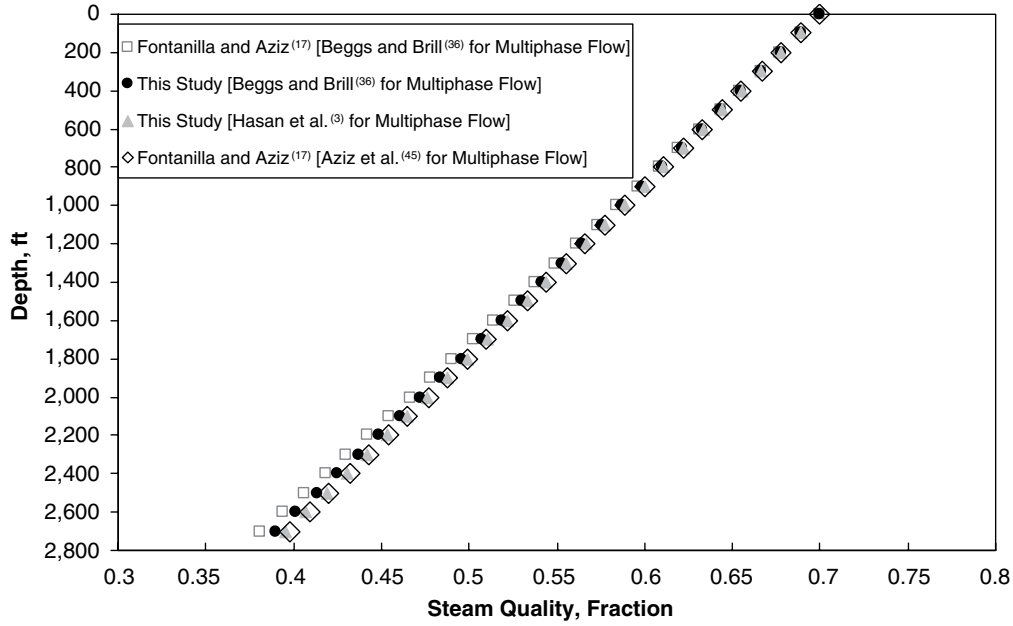

Fig. 23—Comparison of predicted steam quality with other models for Field Test 3A after 16 hours of steam injection.

$in.^2$ × 6.451 6*	E+00 =	cm^2
lbf × 4.44822	E+00 =	N
lbm × 4.535924	E−01 =	kg
psi × 6.894 757	E+00 =	kPa
psia × 6.894757	E+00 =	kPa

*Conversion factor is exact.

References

1. Schlumberger, M., Doll, G.H., and Perebinossoff, A.A. 1937. Temperature Measurements in Oil Wells. *Journal of the Institute of Petroleum Technologists* **23** (159): 1–20.
2. Nowak, T.J. 1953. The Estimation of Water Injection Profiles From Temperature Surveys. SPE-953203-G. *Trans.*, AIME, **198**: 203–212.
3. Bird, J.M. 1954. Interpretation of Temperature Logs in Water- and Gas-Injection Wells and Gas-Producing Wells. *API Drilling and Production Practice* (1954): 187–195. Paper No. 54-187.]
4. Lesem, L.B., Greytok, F., Marotta, F., and McKetta, J.J. Jr. 1957. A Method of Calculating the Distribution of Temperature in Flowing Gas Wells. *Trans.,* AIME, **210**: 169–176. SPE-767-G.
5. Kirkpatrick, C.V. 1959. Advances in Gas-Lift Technology. *API* Drilling and Production Practice (1959): 24–60. Paper No. 54-024.
6. Moss, J.T. and White, P.D. 1959. How to Calculate Temperature Profile in a Water-Injection Well. *Oil & Gas Journal* **57** (11): 174–178.
7. Ramey, H.J. Jr. 1962. Wellbore Heat Transmission. *J Pet Technol* **14** (4): 427–435; *Trans.*, AIME, **225**. SPE-96-PA. doi: 10.2118/96-PA.
8. Edwardson, M.J., Girner, H.M., Parkinson, H.R., Williams, C.D., and Matthews, C.S. 1962. Calculation of Formation Temperature Disturbances Caused by Mud Circulation. *J Pet Technol* **14** (4): 416–426. SPE-124-PA. doi: 10.2118/124-PA.

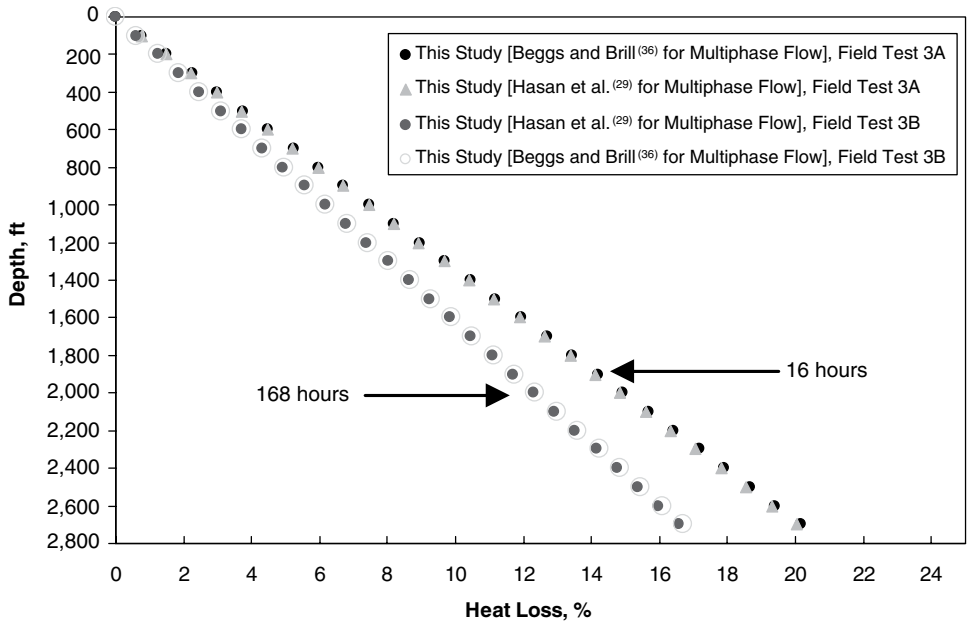

Fig. 24—Prediction of cumulative heat loss for Field Tests 3A and 3B after 16 and 168 hours of steam injection, respectively.

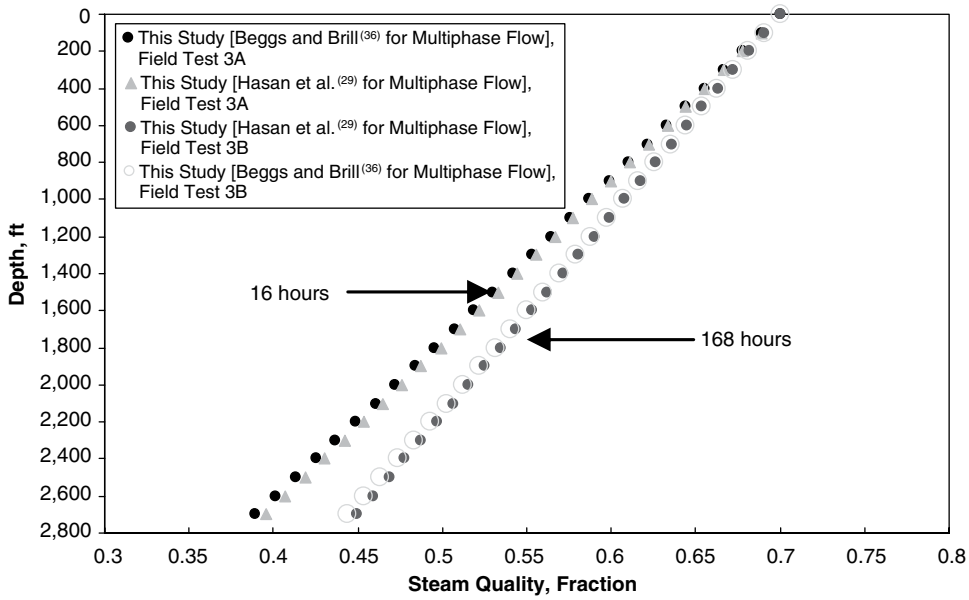

Fig. 25—Prediction of steam quality for Field Tests 3A and 3B after 16 and 168 hours of steam injection, respectively.

9. Bahonar, M., Azaiez, J., and Chen, Z. 2010. A Semi-Unsteady-State Wellbore Steam/Water Flow Model for Prediction of Sandface Conditions in Steam Injection Wells. *J Can Pet Technol* **49** (9): 13–21. SPE-140663-PA. doi: 10.2118/140663-PA.
10. Satter, A. 1965. Heat Losses During Flow of Steam Down a Wellbore. *J Pet Technol* **17** (7): 845–851; *Trans.,* AIME, **234**. SPE-1071-PA. doi: 10.2118/1071-PA.
11. Holst, P.H. and Flock, D.L. 1966. Wellbore Behavior during Saturated Steam Injection. *J Can Pet Technol* **5** (4): 184–193. JCPT Paper No. 66-04-05. doi: 10.2118/66-04-05.
12. Willhite, G.P. 1967. Over-all Heat Transfer Coefficients in Steam and Hot Water Injection Wells. *J Pet Technol* **19** (5): 607–615. SPE-1449-PA. doi: 10.2118/1449-PA.
13. Pacheco, E.F. and Ali, F.S.M. 1972. Wellbore Heat Losses and Pressure Drop in Steam Injection. *J Pet Technol* **24** (2): 139–144. SPE-3428-PA. doi: 10.2118/3428-PA.
14. Herrera, J.O. Jr., George, W.D., Birdwell, B.F., and Hanzlik, E.J. 1978. Wellbore Heat Losses in Deep Steam Injection Wells S1-B Zone, Cat Canyon Field. Paper SPE 7117 presented at the SPE California Regional Meeting, San Francisco, 12–14 April. doi: 10.2118/7117-MS.
15. Shiu, K.C. and Beggs, H.D. 1980. Predicting Temperatures in Flowing Oil Wells. *J. Energy Resour. Technol.* **102** (1): 2–11. doi: 10.1115/1.3227845.
16. Ali, F.S.M. 1981. A Comprehensive Wellbore Stream/Water Flow Model for Steam Injection and Geothermal Applications. *SPE J.* **21** (5): 527–534. SPE-7966-PA. doi: 10.2118/7966-PA.
17. Fontanilla, J.P. and Aziz, K. 1982. Prediction of Bottom-Hole Conditions for Wet Steam Injection Wells. *J Can Pet Technol* **21** (2): 82–88. JCPT Paper No. 82-02-04. doi: 10.2118/82-02-04.
18. Yao, S.C. 1985. Fluid Mechanics and Heat Transfer in Steam Injection Wells. MS thesis, University of Tulsa, Tulsa, Oklahoma.

19. Hong, K.C. and Griston, S. 1986. New Methods for Controlled Injection of Steam Into Multiple Sands. Paper SPE 15472 presented at the SPE Annual Technical Conference and Exhibition, New Orleans, 5–8 October. doi: 10.2118/15472-MS.
20. Griston, S. and Willhite, G.P. 1987. Numerical Model for Evaluating Concentric Steam Injection Wells. Paper SPE 16337 presented at the SPE California Regional Meeting, Ventura, California, USA, 8–10 April. doi: 10.2118/16337-MS.
21. Sharma, Y., Shoham, O., and Brill, J.P. 1989. Simulation of Downhole Heater Phenomena in the Production of Wellbore Fluids. *SPE Prod Eng* **4** (3): 309–312. SPE-16904-PA. doi:10.2118/16904-PA.
22. Stone, T.W., Edmund, N.R., and Kristoff, B.J. 1989. A Comprehensive Wellbore/Reservoir Simulator. Paper SPE 18419 presented at the SPE Symposium on Reservoir Simulation, Houston, 6–8 February. doi: 10.2118/18419-MS.
23. Wu, Y.S. and Pruess, K. 1990. An Analytical Solution for Wellbore Heat Transmission in Layered Formations. *SPE Res Eng* **5** (4): 531–538. SPE-17497-PA. doi: 10.2118/17497-PA.
24. Sagar, R.K., Doty, D.R., and Schmidt, Z. 1991. Predicting Temperature Profiles in a Flowing Well. *SPE Prod Eng* **6** (6): 441–448. SPE-19702-PA. doi: 10.2118/19702-PA.
25. Alves, I.N., Alhanati, F.J.S., and Shoham, O. 1992. A Unified Model for Predicting Flowing Temperature Distribution in Wellbores and Pipelines. *SPE Prod Eng* **7** (6): 363–367. SPE-20632-PA. doi: 10.2118/20632-PA.
26. Hagoort, J. 2004. Ramey's Wellbore Heat Transmission Revisited. *SPE J.* **9** (4): 465–474. SPE-87305-PA. doi: 10.2118/87305-PA.
27. Hasan, A.R. and Kabir, C.S. 1994. Aspects of Wellbore Heat Transfer During Two-Phase Flow. *SPE Prod & Fac* **9** (3): 211–216. SPE-22948-PA. doi: 10.2118/22948-PA.
28. Hasan, A.R. and Kabir, C.S. 2002. *Fluid Flow and Heat Transfer in Wellbores*. Richardson, Texas: Textbook Series, SPE.
29. Hasan, A.R., Kabir, C.S., and Lin, D. 2005. Analytic Wellbore-Temperature Model for Transient Gas-Well Testing. *SPE Res Eval & Eng* **8** (1): 240–247. SPE-84288-PA. doi: 10.2118/84288-PA.
30. Hasan, A.R. and Kabir, C.S. 2009. Modeling Two-Phase Fluid and Heat Flows in Geothermal Wells. Paper SPE 121351 presented at the SPE Western Regional Meeting, San Jose, California, USA, 24–26 March. doi: 10.2118/121351-MS.
31. Hasan, A.R., Kabir, C.S., and Wang, X. 2009. A Robust Steady-State Model for Flowing-Fluid Temperature in Complex Wells. *SPE Prod & Oper* **24** (2): 269–276. SPE-109765-PA. doi: 10.2118/109765-PA.
32. Livescu, S., Durlofsky, L.J., Aziz, K., and Ginestra, J.C. 2009. A fully-coupled thermal multiphase wellbore flow model for use in reservoir simulation. *J. Pet. Sci. Eng*. (in press; published online 03 December 2009). doi:10.1016/j.petrol.2009.11.022.
33. Livescu, S., Aziz, K., and Durlofsky, L.J. 2009. Development and Application of a Fully-Coupled Thermal Compositional Wellbore Flow Model. Paper SPE 121306 presented at the SPE Western Regional Meeting, San Jose, California, USA, 24–26 March. doi: 10.2118/121306-MS.
34. Stone, T.W., Bennett, J., Law, D.H.-S., and Holmes, J.A. 2002. Thermal Simulation with Multisegment Wells. *SPE Res Eval & Eng* **5** (3): 206–218. SPE-78131-PA. doi: 10.2118/78131-PA.
35. Pourafshary, P., Varavei, A., Sepehrnoori, K., and Podio, A. 2008. A Compositional Wellbore/Reservoir Simulator to Model Multiphase Flow and Temperature Distribution. Paper SPE 12115 presented at the International Petroleum Technology Conference, Kuala Lampur, 3–5 December. doi: 10.2523/12115-MS.
36. Beggs, H.D. and Brill, J.P. 1973. A Study of Two-Phase Flow in Inclined Pipes. *J Pet Technol* **25** (5): 607–617; *Trans.*, AIME, **255**. SPE-4007-PA. doi: 10.2118/4007-PA.
37. Hasan, A.R., Kabir, C.S., Sayarpour, M. 2007. A Basic Approach to Wellbore Two-Phase Flow Modeling. Paper SPE 109868 presented at the SPE Annual Technical Conference and Exhibition, Anaheim, California, USA, 11–14 November. doi: 10.2118/109868-MS.
38. Livescu, S., Durlofsky, L.J., and Aziz, K. 2008. Application of a New Fully-Coupled Thermal Multiphase Wellbore Flow Model. Paper SPE 113215 presented at the SPE/DOE Symposium on Improved Oil Recovery, Tulsa, Oklahoma, USA, 20–23 April. doi: 10.2118/113215-MS.
39. Livescu, S., Durlofsky, L.J., and Aziz, K. 2008. A Semianalytical Thermal Multiphase Wellbore Flow Model for Use in Reservoir Simulation. Paper SPE 115796 presented at the SPE Annual Technical Conference and Exhibition, Denver, 21–24 September. doi: 10.2118/115796-MS.
40. Wang, X. 1996. Modeling Coupled Transient Transport of Mass, Momentum and Energy in Wellbore/Reservoir Systems. PhD dissertation, University of North Dakota, Grand Forks, North Dakota.
41. Horne, R.N. and Shinohara, K. 1979. Wellbore Heat Loss in Production and Injection Wells. *J Pet Technol* **31** (1): 116–118. SPE-7153-PA. doi: 10.2118/7153-PA.
42. Fontanilla, J.P. 1980. A Mathematical Model for the Prediction of Wellbore Heat Loss and Pressure Drop in Steam Injection Wells. MS thesis, University of Calgary, Calgary, Alberta.
43. Carslaw, H.S. and Jaeger, J.C. 1950. *Conduction of Heat in Solids*. Oxford, UK: Oxford University Press.
44. Bleakley, W.B. 1964. Here are case histories of two thermal projects (Thermal Recovery: Second of Two Installments). *The Oil and Gas Journal* (October 26, 1964): 123–130.
45. Aziz, K., Govier, G.W., and Fogarasi, M. 1972. Pressure Drop in Wells Producing Oil and Gas. *J Can Pet Technol* **11** (3): 38–48. JCPT Paper No. 72-03-04. doi:10.2118/72-03-04.

Appendix A

Coefficients of Equation (18):

$$\alpha_L = 2\alpha'_{e_{k,i}}\Delta t^{n+1}\times\left[k_{ez_{k-\frac{1}{2},i}}\frac{1}{\Delta z_k}\left(\frac{1}{\Delta z_{k-1}+\Delta z_k}\right)\right], \quad \text{..... (1A)}$$

$$\alpha_W = 2\alpha'_{e_{k,i}}\Delta t^{n+1}\times\left[k_{er_{k,i-\frac{1}{2}}}\frac{r_{i-\frac{1}{2}}}{r_i}\frac{1}{\Delta r_i}\left(\frac{1}{\Delta r_{i-1}+\Delta r_i}\right)\right], \quad \text{..... (2A)}$$

$$\alpha_C = -2\alpha'_{e_{k,i}}\Delta t^{n+1}\times\left[\begin{array}{l} k_{er_{k,i+\frac{1}{2}}}\dfrac{r_{i+\frac{1}{2}}}{r_i}\dfrac{1}{\Delta r_i}\left(\dfrac{1}{\Delta r_{i+1}+\Delta r_i}\right) \\ +k_{er_{k,i-\frac{1}{2}}}\dfrac{r_{i-\frac{1}{2}}}{r_i}\dfrac{1}{\Delta r_i}\left(\dfrac{1}{\Delta r_{i-1}+\Delta r_i}\right) \\ +k_{ez_{k+\frac{1}{2},i}}\dfrac{1}{\Delta z_k}\left(\dfrac{1}{\Delta z_{k+1}+\Delta z_k}\right) \\ +k_{ez_{k-\frac{1}{2},i}}\dfrac{1}{\Delta z_k}\left(\dfrac{1}{\Delta z_{k-1}+\Delta z_k}\right) \\ +\dfrac{1}{2\alpha'_{e_{k,i}}\Delta t^{n+1}} \end{array}\right], \quad \text{..... (3A)}$$

$$\alpha_E = 2\alpha'_{e_{k,i}}\Delta t^{n+1}\times\left[k_{er_{k,i+\frac{1}{2}}}\frac{r_{i+\frac{1}{2}}}{r_i}\frac{1}{\Delta r_i}\left(\frac{1}{\Delta r_{i+1}+\Delta r_i}\right)\right], \quad \text{..... (4A)}$$

$$\alpha_U = 2\alpha'_{e_{k,i}}\Delta t^{n+1}\times\left[k_{ez_{k+\frac{1}{2},i}}\frac{1}{\Delta z_k}\left(\frac{1}{\Delta z_{k+1}+\Delta z_k}\right)\right] \quad \text{..... (5A)}$$

Appendix B

The location of grid boundaries and centres for geometric gridding system are given as follows:

$$\beta = \left(\frac{r_e}{r_{wb}}\right)^{\frac{1}{NoGrid}}, \quad \text{..... (1B)}$$

$$r_{i+\frac{1}{2}} = \beta \times r_{i-\frac{1}{2}}, \text{ i=1, 2, …, Number of Grids, } r_{1/2}, = r_{wb} \quad \text{..... (2B)}$$

$$r_i = \sqrt{r_{i+1/2} \times r_{i-1/2}}, \text{ i=1, 2, …, Number of Grids, } \quad \text{..... (3B)}$$

$$\Delta r_i = r_{i+1/2} - r_{i-1/2}, \text{ i=1, 2, …, Number of Grids, } \quad \text{..... (4B)}$$

$$r_{i+\frac{1}{2}} = \sqrt{r_i r_{i+1}}, \; r_{i-\frac{1}{2}} = \sqrt{r_i r_{i-1}}, \; r_{1-\frac{1}{2}} = r_{wb} \quad \text{..... (5B)}$$

Authors

Mehdi Bahonar is a petroleum engineering Ph.D. candidate who joined the Department of Chemical and Petroleum Engineering at the University of Calgary in September 2007. Bahonar has conducted research that explains topics related to steam injection in a fractured heavy oil carbonate reservoir in Iran, natural convection and thermal radiation in wellbore annulus and is currently looking at the modelling of transient nonisothermal fluid flow and heat transfer in coupled wellbore/reservoir systems. Bahonar has received several academic awards, scholarships and bursaries (including the Alberta Ingenuity Ph.D. Graduate Student Scholarship) and authored or coauthored a number of technical and journal papers. He holds a B.Sc. degree in petroleum production engineering from the Petroleum University of Technology (PUT) in Iran and dual-M.Sc./M.Eng. degrees in reservoir engineering from the University of Calgary/PUT. He is a member of SPE and APEGGA.

Jalel Azaiez is currently an associate professor at the Department of Chemical and Petroleum Engineering in the University of Calgary. Azaiez' expertise is in the field of mathematical modelling and numerical simulation of fluid flows with a particular focus on complex systems. These include non-Newtonian fluids flows, rheological modelling of fibre and polymer systems, viscous fingering and other chemically or thermally driven instabilities in porous media. He has published more than 40 refereed journal papers, more than 20 refereed conference proceedings papers and has given 55 conference presentations. He has also presented nine invited talks and seminars worldwide. He holds a Dilôme d'Ingénieur from the Ecole Centrale de Paris in France and M.Sc. and Ph.D. degrees from Stanford University.

Zhangxin (John) Chen is currently a professor at the University of Calgary, director of Schlumberger iCentre for Simulation & Visualization and holds the NSERC/AERI/Foundation CMG Senior Research Chair in Reservoir Simulation and iCORE Industrial Chair in Reservoir Modelling. He formerly held a Tengfei Chaired and Chang Jiang Chaired Professorship at Xi'an Jiaotong University, Tepin Professorship of Energy and Resources at the Peking University, Ziqiang Professorship at Shanghai University and Gerald J. Ford Research Professorship at Southern Methodist University. His research interest is in numerical reservoir simulation, high-performance computing, mathematical modelling and algorithm development. He holds a B.S. degree from the University of Jiangxi, an M.S. degree from Xi'an Jiaotong University in China and a Ph.D. degree from Purdue University.